lncRNA *DIGIT* and BRD3 protein form phase-separated condensates to regulate endoderm differentiation

Kaveh Daneshvar[1,2], **M. Behfar Ardehali**[3,4], **Isaac A. Klein**[5,6], **Fu-Kai Hsieh**[3,4], **Arcadia J. Kratkiewicz**[1,2], **Amin Mahpour**[1,2], **Sabrina O.L. Cancelliere**[2,7], **Chan Zhou**[1,2], **Brett M. Cook**[8], **Wenyang Li**[1,2], **Joshua V. Pondick**[1,2], **Sweta K. Gupta**[1,2], **Sean P. Moran**[1,2], **Richard A. Young**[5,9], **Robert E. Kingston**[3,4], **Alan C. Mullen**[1,2,7,*]

[1]Gastrointestinal Unit, Massachusetts General Hospital, Boston, MA 02114, USA

[2]Harvard Medical School, Boston, MA 02115, USA

[3]Department of Molecular Biology and MGH Research Institute, Massachusetts General Hospital, Boston, MA 02114, USA

[4]Department of Genetics, Harvard Medical School, Boston, MA 02115, USA

[5]Whitehead Institute for Biomedical Research, Cambridge, MA 02142, USA

[6]Department of Medical Oncology, Dana-Farber Cancer Institute, Harvard Medical School, Boston, MA 02215, USA

[7]Harvard Stem Cell Institute, Cambridge, MA 02138, USA

[8]Optical Biosystems, Inc. Santa Clara, CA 95050, USA

[9]Department of Biology, Massachusetts Institute of Technology, Cambridge, MA 02139, USA

Abstract

Cooperation between DNA, RNA and protein regulates gene expression and controls differentiation through interactions connecting regions of nucleic acids and protein domains and through the assembly of biomolecular condensates. Here, we report that endoderm differentiation is regulated through the interaction of the long noncoding (lnc) RNA *DIGIT* and the bromodomain and extra-terminal domain protein BRD3. BRD3 forms phase-separated condensates, the formation of which are promoted by *DIGIT*, occupies enhancers of endoderm transcription factors, and is required for endoderm differentiation. BRD3 binds acetylated histone H3 lysine 18 (H3K18ac) *in vitro* and co-occupies the genome with H3K18ac. *DIGIT* is also enriched in regions

[*]Corresponding author. Thier 306B, 55 Fruit Street, Massachusetts General Hospital, Boston, MA 02114, USA. (617) 726-6342. acmullen@mgh.harvard.edu.

of H3K18ac, and depletion of *DIGIT* results in decreased recruitment of BRD3 to these regions. Our findings show that cooperation between *DIGIT* and BRD3 at regions of H3K18ac regulates the transcription factors that drive endoderm differentiation and suggest a broader role for protein-lncRNA phase-separated condensates as regulators of transcription.

Introduction

Gene expression programs that determine cell identity are regulated by interactions between DNA, RNA and protein, and these programs change during differentiation as new interactions are created and previous interactions fall apart. Long noncoding RNAs are components of the circuitry that control embryonic stem cell (ESC) pluripotency and differentiation[1–6], and the lncRNA *DIGIT* regulates definitive endoderm differentiation[4].

We find that *DIGIT* interacts with BRD3, a member of the bromodomain and extra-terminal (BET) domain family of proteins. BET proteins contain two bromodomains, which bind acetylated histones[7,8], and an extra-terminal domain that enables interaction with other proteins, including transcription factors and co-activators[9–12]. BRD2, BRD3 and BRD4 are BET family proteins that are ubiquitously expressed and have unique functions in development. *Brd4*^{−/−} embryos die before implantation[13], and *Brd2*^{−/−} embryos die between E9.5 and E11.5[14]. BRD4 regulates pluripotency and self-renewal of murine ESCs[15], while BRD2 promotes expression of Nodal when ESCs are released from pluripotency[16]. Different functions of BET proteins in ESCs are associated with different patterns of genome occupancy, where BRD4 is enriched at enhancers, while BRD2 and BRD3 are enriched at promoters[15]. Furthermore, BRD4 forms phase-separated droplets in murine ESCs, which have been proposed to promote the recruitment of transcription machinery[17]. While critical roles for BRD2 and BRD4 have been established in early development, the function of BRD3 is unclear.

Here we report that *DIGIT* interacts with BRD3 and promotes the formation of phase-separated condensates during endoderm differentiation. With differentiation, BRD3 occupies new sites at endoderm genes, many of which are also regulated by *DIGIT*. Recombinant BRD3 binds H3K18ac, and BRD3 co-occupies the genome with H3K18ac. *DIGIT* is enriched at sites of H3K18ac, and depletion of *DIGIT* reduces BRD3 occupancy at these sites. We propose that BRD3 is recruited to sites of H3K18ac to form phase-separated condensates and promote transcription, and BRD3 recruitment and condensate formation is dependent on *DIGIT*. Through this process, the interaction between *DIGIT* and BRD3 at sites of H3K18ac activates genes that regulate endoderm differentiation.

Results

Design of an aptamer-based approach to define the DIGIT-protein interactome

We fused the 3' end of *DIGIT* cDNA to four copies of an aptamer with high affinity for streptavidin (4xS1m)[18,19]. We confirmed that the *DIGIT-4xS1m* transcript was retained in the nucleus after transient transfection (Figure 1A), as previously described for endogenous *DIGIT*[4], and precipitated *DIGIT-4xS1m* with streptavidin beads in UV cross-linked cells

(Figure 1B). We then adjusted the potassium chloride concentration in the wash buffer to optimize enrichment of *DIGIT* over *GAPDH* mRNA (Extended Data Figure 1A), resulting in greater than 125-fold enrichment of *DIGIT-4xS1m* after precipitation (Figure 1C). These experiments show that the 4xS1m aptamer can be fused to lncRNAs and used to enrich lncRNAs in UV cross-linked cells.

DIGIT interacts with BRD3

To identify proteins that interact with *DIGIT*, we transiently expressed *DIGIT-4xS1m* in hESCs and differentiated toward endoderm. As controls, we ectopically expressed a scrambled form of *DIGIT* fused to 4xS1m (*SCRM-4xS1m*) (Extended Data Figure 1B) and the *DIGIT* transcript without 4xS1m. We performed UV cross-linking followed by streptavidin precipitation and mass spectrometry (MS). BRD3 showed the highest interaction score (Figure 1D and Table S1), and the interaction was confirmed by streptavidin precipitation followed by immunoblotting to detect BRD3 protein (Figure 1E).

It is possible that an increase in the number of *DIGIT* molecules present with ectopic expression could lead to interactions that are not formed with endogenous *DIGIT*. To validate the interaction of BRD3 with endogenous *DIGIT*, we performed RNA-immunoprecipitation (RIP) in nuclear lysates from endoderm cells (Extended Data Figure 1C and 1D) using an antibody against BRD3, which demonstrated a 6-fold increase in *DIGIT* compared to RNA precipitated with IgG (Figure 1F). Enrichment of *DIGIT* was also greater than enrichment measured for eleven other RNA transcripts. For this analysis, we included the lncRNAs *DEANR1* and *GATA6-AS20*. *GATA6-AS* has not been evaluated in endoderm differentiation. Therefore, we defined the 5′- and 3′-ends of *GATA6-AS* by Rapid Amplification of cDNA Ends (RACE), cloned the full-length cDNA from endoderm cells (Extended Data Figure 1E) and quantified expression with differentiation (Extended Data Figure 1F) to define the *GATA6-AS* transcript that is induced upon endoderm differentiation. These experiments confirm that endogenous BRD3 interacts with endogenous *DIGIT* and reveals that BRD3 preferentially binds *DIGIT* compared to selected RNA transcripts.

SMARCD1, a component of the SWI/SNF chromatin remodeling complex[21], which is involved in embryonic stem cell differentiation[22], was also identified to interact with *DIGIT* (Figure 1D). Endogenous *DIGIT* associates with SMARCD1 (Extended Data Figure 2A), and SMARCD1 interacts with BRD3 (Extended Data Figure 2B). Future studies are needed to determine if *DIGIT*, BRD3 and SMARCD1 are present in the same complex.

To understand how BRD3 interacts with the entire transcriptome, we performed RIP using an antibody against BRD3 followed by sequencing of precipitated RNA. *DIGIT* was enriched with precipitation of BRD3, whether compared to total nuclear RNA (input) or to RIPs using IgG as a control (Figure 1G). Furthermore, we found that *DIGIT* was one of the most enriched transcripts with BRD3 RIP (Figure 1H, Extended Data Figure 2C, left and Extended Data Figure 2D, left, Table S1). These results provide further evidence that BRD3 binds *DIGIT* and reveal that BRD3 also interacts with other coding and noncoding RNAs in both endoderm and hESCs (Extended Data Figure 2C and 2D, Table S1).

BRD3 shows specificity for DIGIT compared to BRD2 and BRD4

BRD2, BRD3 and BRD4 but not BRDT are expressed in endoderm cells (Extended Data Figure 2E), and we asked if the other BET proteins interact with *DIGIT*. We again observed an enrichment of *DIGIT* with precipitation of BRD3. However, recovery of *DIGIT* was reduced with precipitation of BRD2 or BRD4 (Figure 1I and Extended Data Figure 2F), suggesting that BRD3 may preferentially interact with *DIGIT* compared to either BRD2 or BRD4.

DIGIT interacts with BRD3 in gel shift assays

To further evaluate the interaction between *DIGIT* and BRD3, we performed gel electrophoresis mobility shift assays (EMSA) with recombinant BRD3 fused to monomeric (m) EGFP and either *DIGIT* or *SCRM*. BRD3 and *DIGIT* formed multiple distinct shifted bands (Figure 2A, red arrows, Extended Data Figure 3A and 3B), consistent with a multivalent mode of interaction[23], and these distinct shifted bands were weaker with BRD3 and *SCRM*. The dissociation constant (K_d) was lower for BRD3-*DIGIT* than BRD3-*SCRM* (K_d = 26.4 nM versus K_d = 46.3 nM) (Figure 2B), and quantification of the shift for *DIGIT* and *SCRM* at the BRD3 concentrations flanking the K_d values also demonstrates a stronger shift for *DIGIT* (Figure 2C). We found similar results in a repeat experiment (Extended Data Figure 3C and 3D). With increasing amounts of RNA, BRD3 showed accelerated migration whether the RNA was *DIGIT* or *SCRM* (Figure 2D, left). However, the relative amount of labeled RNA that migrates with BRD3 is higher for *DIGIT* than *SCRM* at each concentration (Figure 2D, right and 2E). These results suggest that *DIGIT* interacts with BRD3 with higher affinity and partitions more stably within the RNA-protein complex than a scrambled RNA of the same length and nucleotide composition.

DIGIT interacts with BRD3 bromodomains

We evaluated the ability of the bromodomains (BD1 and BD2) and extra-terminal (ET) domain of BRD3 to interact with RNA and with *DIGIT*. We first performed Orthogonal Organic Phase Separation (OOPS)[24] and determined that full-length BRD3, BD1, BD1/BD2 and the ET domain, but not mEGFP, interact with RNAs (Figure 2F and 2G, Extended Data Figure 3E and 3F). In contrast, only BD1 and BD1/BD2 interact with *DIGIT* (Figure 2H). Thus while both bromodomains and ET domains can interact with RNA, only the bromodomains of BRD3 interact with *DIGIT*.

DIGIT localizes within BRD3 puncta

We next visualized *DIGIT* and BRD3 within the nuclei of endoderm cells. Images revealed that BRD3 is not evenly distributed through the nucleus, and instead forms puncta (Figure 3A, center), a phenomenon that has been described for BRD4[17]. The analysis also revealed multiple sites of overlap between BRD3 and *DIGIT* (Figure 3A, left), suggesting that *DIGIT* transcripts localize to these puncta and we are not simply observing sites of *DIGIT* transcription inside the puncta.

Eighteen percent of *DIGIT* transcripts overlap with BRD3, and this overlap is significantly higher than the overlap observed between BRD3 and *GSC* mRNA (<1%) (Figure 3B). For this analysis, we focused only on transcripts localized to the nucleus for both *DIGIT* (379)

and *GSC* mRNA (2412). *DIGIT* transcripts are more likely to localize to larger BRD3 puncta compared to *GSC* (Figure 3C). We previously observed that *DIGIT* was preferentially enriched with precipitation of BRD3 compared to BRD2 and BRD4 (Figure 1I). To exclude the possibility that the affinity or epitope for an individual antibody may have affected interpretation of these results, we quantified the overlap between puncta for each BET protein and *DIGIT* in endoderm cells (Figure 3B). We observed that a lower percentage of *DIGIT* molecules overlap with BRD2 (4.4%) and BRD4 (3.5%), compared to BRD3 (18%). These results suggest that *DIGIT* preferentially interacts with BRD3 puncta.

BRD3 shows properties of liquid-liquid phase-separated condensates

Seventy-five percent of the long isoform of BRD3 and 67% of the short isoform of BRD3 are disordered (Extended Data Figure 4A), and intrinsically disordered regions have been linked to the formation of phase-separated condensates[25–27]. To investigate whether BRD3 puncta are phase-separated condensates, we first asked if BRD3 forms condensates in live cells. We used the CRISPR/Cas system to insert mEGFP cDNA into the 5′ end of the endogenous *BRD3* gene (Extended Data Figure 4B and 4C). The generation of fused mEGFP-BRD3 was confirmed by immunoblot (Extended Data Figure 4D), and confocal microscopy demonstrated the formation of BRD3 puncta in both live and fixed endoderm cells (Figure 3D). Expression of mEGFP alone did not lead to puncta formation. To test whether BRD3 puncta display rapid exchange kinetics with their surroundings, which is characteristic of phase separated condensates[17,28,29], we performed Fluorescence Recovery After Photobleaching (FRAP). BRD3-mEGFP puncta are able to recover up to 20% fluorescence in 10 seconds and up to 38% fluorescence in 30 seconds (Figure 3E and 3F). These results show that BRD3 molecules form puncta with properties consistent with liquid-liquid phase-separated condensates.

BRD3 forms phase-separated condensates in hESCs and with endoderm differentiation (Figure 3D–3F, and Extended Data Figure 4E). BRD4 forms condensates in mESCs[17], and BRD2, BRD3 and BRD4 all have large domains of predicted disorder (Extended Data Figure 4A). All three proteins form puncta with endoderm differentiation, and BRD3 puncta are separate from those composed of BRD4 or BRD2 (Figure 3G). These findings demonstrate that each BET protein forms nuclear condensates in definitive endoderm, and the condensates formed by BRD3 are distinct from those formed by BRD2 and BRD4.

BRD3 forms condensates in vitro

Proteins that compose phase-separated biomolecular condensates may form liquid droplets *in vitro* [30]. A titration of recombinant BRD3 fused to mEGFP begins to form droplets at a concentration between 1 and 5 μM (Figure 4A). Phase-separated droplets, which rely on electrostatic interactions, are sensitive to salt, so we asked if BRD3 forms droplets at physiologic salt concentrations. A titration of sodium chloride (NaCl) showed that BRD3 forms droplets at concentrations as high as 300 mM (Figure 4B). To confirm that *in vitro* formation of BRD3 droplets is not uniquely observed in the presence of the macromolecular crowding agent polyethylene glycol (10% PEG-8000), we tested the formation of droplets in the presence of three other crowding agents: PEG-6000 (10%), Ficoll 400 (10%) and bovine serum albumin (BSA, 15%) (Extended Data Figure 4F).

DIGIT nucleates BRD3 condensates

We next asked if BRD3 droplets formed *in vitro* interact with *DIGIT*. We synthesized Cy3-labeled *DIGIT* (Extended Data Figure 4G) and induced *in vitro* formation of BRD3 droplets in the presence of Cy3-*DIGIT*. We observed that the Cy3-*DIGIT* molecules were concentrated within BRD3 droplets (Figure 4C), while Cy3-*DIGIT* molecules alone remain dispersed (Figure 4C, far right), suggesting that BRD3 forms phase-separated condensates that contain *DIGIT in vitro*.

Titration of BRD3 in a low concentration of crowding agent (1.5% PEG-6000) and in the presence of *in vitro* transcribed *DIGIT* showed the formation of BRD3 droplets at 0.5 μM (Figure 4D), a concentration at which BRD3 droplets do not form on their own (Figure 4A). The equivalent intensity of droplet formation was not observed under these conditions until a BRD3 concentration of greater than 1 μM in the presence of *SCRM* or in the absence of RNA (Figure 4D). Tracking droplet formation and RNA localization for *DIGIT* and *SCRM* demonstrated that *DIGIT* promotes droplet formation and is concentrated within these droplets (Figure 4E). These findings demonstrate a sequence-specific role for *DIGIT* in promoting the formation of BRD3 condensates *in vitro*.

To determine if the local concentration of *DIGIT* within cells promotes the formation of BRD3 condensates, we generated hESCs that stably express either *DIGIT* or GFP at multiple sites using the Sleeping Beauty system[31]. We chose GFP RNA as a negative control because this transcript is also not expressed in hESCs. Sequential RNA-FISH and IF revealed BRD3 condensates in regions of increased concentration of *DIGIT* but not in regions of increased concentration of *GFP* mRNA (Figure 4F). These results suggest *DIGIT* promotes the formation of BRD3 condensates both *in vitro* and in cells.

BRD3 regulates definitive endoderm differentiation

BRD3 is dispensable for the maintenance of ESC pluripotency[15], but its role in endoderm differentiation is unknown. We generated homozygous hESC lines deficient in BRD3 (*BRD3*−/−) (Figure 5A and Extended Data Figure 5A) by inserting a puromycin (puro) resistance cassette followed by a stop codon after the sixth amino acid of BRD3. mRNA levels of *OCT4* and *NANOG* show no statistically significant changes between *BRD3*−/− hESCs and control cells (Figure 5B), suggesting that pluripotency is not significantly affected by the loss of BRD3. However, *BRD3*−/− hESCs demonstrate a defect in endoderm differentiation as quantified by expression of *SOX17* and *CXCR4* mRNA (Figure 5C) and co-expression of CXCR4 and c-KIT (Figure 5D).

We next evaluated the requirement of BRD3 under differentiation conditions that produce ectoderm, mesoderm, and endoderm[32,33]. Treatment of hESCs on micropatterned slides with BMP4 induces spatially organized differentiation, with ectoderm (SOX2) in the central region, definitive endoderm (SOX17) on the periphery, and mesoderm between ectoderm and endoderm. *BRD3*−/− cells showed reduced SOX17 expression on the periphery of differentiating colonies as well as an expansion of SOX2-positive cells in the center (Figure 5E), demonstrating that loss of BRD3 inhibits endoderm differentiation, a phenotype also observed with depletion of *DIGIT*[4].

BRD3 encodes both short and long isoforms. Loss of function analysis and studies of the tagged endogenous BRD3 protein were designed to deplete (Figure 5A) and tag both isoforms (Extended Data Figure 4B), and thus do not distinguish between isoforms. Using primers specific for each isoform, we found that only the long isoform is detected with endoderm differentiation (Extended Data Figure 5B). However, ectopic expression of the long and short isoforms are each capable of rescuing expression of genes that mark endoderm cell fate (Extended Data Figure 5C), suggesting overlapping function between the two isoforms even though the long isoform is the predominant form in endoderm.

BRD3 interacts with acetylated H3K18

Individual bromodomains of BRD3 interact with acetylated histones[8], but the affinity of full-length BRD3 for modified histones has not been investigated. We found that both long and short isoforms of BRD3 show the strongest interaction with H3K18ac (Figure 6A, 6B, Extended Data Figure 6A, and 6B) (Table S2). The long isoform of BRD3 also shows slightly weaker binding to H4K20ac and H2AK13ac and the short isoform to H4K8ac and H4K20ac (Figure 6B and Extended Data Figure 6B). To evaluate the interaction between H3K18ac and BRD3 further, we asked if H3K18ac affects BRD3 occupancy at known target genes. H3K18ac is produced by CBP/p300, which is also responsible for H3K27ac[34]. We treated hESCs with A485, which inhibits both H3K18ac and H3K27ac[35], and with GNE049, which inhibits only H3K27ac[35,36]. BRD3 showed minimal interaction with H3K27ac (Extended Data Figure 6B), and we hypothesized that inhibition of H3K18ac and H3K27ac should have a greater effect on BRD3 occupancy than inhibition of H3K27ac alone. A485 reduced both H3K18ac and H3K27ac (Extended Data Figure 6C), and BRD3 occupancy was significantly reduced at the loci of genes previously identified as occupied by BRD3 in hESCs[15], as compared to hESCs treated with GNE049 (Extended Data Figure 6D). These results suggest that BRD3 binds H3K18ac, prompting further investigation.

BRD3 and H3K18ac co-occupy genes that regulate pluripotency and differentiation

We then asked if the interaction between H3K18ac and BRD3 extends to native chromatin in endoderm differentiation. ChIP-seq analysis showed no evidence of BRD3 or H3K18ac at the *DIGIT/GSC* locus in hESCs. However, BRD3 occupies this locus with endoderm differentiation (Table S3). Mesendoderm gives rise to endoderm, and many endoderm genes are first activated in mesendoderm[37,38]. In mesendoderm, we observed H3K18ac in the same regions that are occupied by BRD3 in endoderm. In contrast, BRD3 occupies regions of H3K18ac in hESCs at the gene encoding the pluripotency factor SOX2, and the presence of both BRD3 and H3K18ac are reduced with endoderm/mesendoderm differentiation (Figure 6D). These findings show that BRD3 and H3K18ac can co-occupy genes in hESCs and shift to new targets with differentiation.

DIGIT is enriched in regions of chromatin modified by H3K18ac

BRD3 localizes to regions of chromatin marked by H3K18ac and interacts with *DIGIT,* suggesting that *DIGIT* may also localize to regions of H3K18ac. We adapted Cleavage Under Targets and Release Using Nuclease (CUT&RUN)[39] to isolate RNA molecules that interact with histone modifications (Cleavage Under Targets and Release Using Nuclease to Assess Enrichment of RNA, CUT&RUNER) (Figure 6E). The CUT&RUN protocol uses

microccocal nuclease (MNase) to excise DNA at targeted regions. MNase can target both DNA and RNA; however, its RNase activity can be inhibited by heavy metal cations (Extended Data Figure 6E and 6F)[40]. We quantified enrichment of the lncRNAs *MALAT1* and *MEG3* as controls. As predicted, *MALAT1* is enriched in regions modified by H3K4me3[41], while *MEG3* is enriched in regions of H3K27me3[42] (Extended Data Figure 6G). We find that *DIGIT* demonstrates the greatest enrichment in regions modified by H3K18ac (Figure 6F). Enrichment of *DIGIT* was also observed to a lesser degree in regions modified by H3K4me3. *GATA6-AS* was enriched in regions of H3K4me3, while *DEANR1* was enriched in regions of H3K18ac but to a lesser degree than *DIGIT*. These results show that BRD3 and *DIGIT* are both enriched in regions of chromatin modified by H3K18ac.

BRD3 promotes gene expression through occupancy of enhancers

BRD3 primarily occupies promoters in hESCs and shows increased occupancy of enhancers with endoderm differentiation (Figure 7A and Extended Data Figure 7A) (Table S4). Key endoderm and mesendoderm genes are occupied by BRD3 and regulated by *DIGIT*. (Figure 7B and 7C). These regulatory genes are also located in regions of higher BRD3 occupancy (Figure 7D). BRD3 regions containing enhancers are also greater in size in endoderm compared to hESCs, in contrast to BRD3 regions containing promoters, which are maintained at similar sizes in endoderm and hESCs (Extended Data Figure 7B). These results suggest that upon endoderm differentiation, BRD3 shifts to occupy new, broader regions that tend to contain enhancers, including those that regulate genes controlling endoderm fate.

It is possible that transcripts such as *DIGIT*, which are expressed from genes that are occupied by BRD3, may show interaction with BRD3 on RIP (Figure 1G) only because there is a higher concentration of the transcript near the gene as it is transcribed. However, we found no association between the level of gene occupancy by BRD3 (ChIP) and enrichment by RIP (Extended Data Figure 7C), suggesting that the interaction of BRD3 and *DIGIT* is regulated more by RNA sequence than the location of transcription relative to BRD3.

BRD3 and H3K18ac are associated across the genome

We next compared sites of H3K18ac in mesendoderm differentiation[43] with BRD3 occupancy during endoderm differentiation. Despite analyzing occupancy under slightly different stages of differentiation, we found that over 80% of regions occupied by BRD3 overlap with regions of H3K18ac (Figure 7E). In both hESCs and with endoderm/mesendoderm differentiation, regions occupied by BRD3 are modified by H3K18ac (Figure 7F and 7G). Approximately 15% of H3K18ac regions are unique in mesendoderm compared to hESCs, and 560 of these mesendoderm regions are newly occupied by BRD3 with endoderm differentiation. This group of genes newly marked by H3K18ac and BRD3 includes the key endoderm genes that are also regulated by *DIGIT* (Figure 7H). These results suggest that during differentiation, BRD3 shifts to regions newly modified by H3K18ac, which encompass genes regulated by *DIGIT*.

DIGIT recruits BRD3 to endoderm genes

The previous results suggest that *DIGIT* may recruit BRD3 to sites of H3K18ac to induce the expression of endoderm genes. We differentiated *DIGIT*-deficient (*DIGIT*^gfp/gfp^) and wildtype hESCs toward endoderm to determine how BRD3 occupancy was affected by depletion of *DIGIT*. *GSC*, *FOXA2* and *SOX17* are co-occupied by BRD3 and H3K18ac (Figure 6C and 7G) and regulated by *DIGIT* (Figure 7B and 7C), and BRD3 occupancy at each of these genes was impaired with *DIGIT* depletion (Figure 8A). We also assessed both BRD3 occupancy at *HEXIM2,* a gene co-occupied by BRD3 and H3K18ac in hESCs and in endoderm but not regulated by *DIGIT* (Extended Data Figure 8), and BRD3 occupancy at *PITX2* and *ZAP70,* genes that show new occupancy by BRD3 and H3K18ac with endoderm differentiation but are not regulated by *DIGIT*. In contrast to *GSC, FOXA2* and *SOX17*, BRD3 occupancy at *HEXIM2, PITX2 and ZAP70* was not reduced (Figure 8B), suggesting that *DIGIT* is required for the recruitment of BRD3 to endoderm genes (Figure 8C).

Discussion

Many lncRNAs interact with proteins to regulate gene expression[44]. Here we demonstrate that *DIGIT* interacts with BRD3 in phase-separated condensates to control gene expression and endoderm differentiation. BRD3 binds H3K18ac, and during endoderm differentiation BRD3 shifts from promoters to enhancers within regions also occupied by H3K18ac. BRD3 can co-occupy genes with H3K18ac independent of *DIGIT* (Figure 8B and Extended Data Figure 8), but BRD3 requires *DIGIT* to occupy regions of H3K18ac near a specific subset of genes (Figure 8A and 8C). Thus, the interaction with *DIGIT* determines the specificity of a set of BRD3 targets, through which BRD3 regulates endoderm differentiation.

In mouse endoderm differentiation, activin signaling leads to increased H3K18ac at the *Gsc* gene[45]. Acetylation of H3K18 at *Gsc* requires both SMAD4 and TRIM33, each of which interacts with SMAD2/3 in response to activin signaling, and H3K18ac may also act to recruit TRIM33[46]. Thus genome occupancy by Smad2/3 at new enhancers may lead to recruitment of CBP/p300[47,48], induction of H3K18ac[34], and recruitment of the BRD3-*DIGIT* complex to drive expression of *Gsc* and other SMAD2/3 target genes.

DIGIT interacts with the bromodomains of BRD3 (Figure 2F), and enhancer (e) RNAs interact with the bromodomains of BRD4[49]. These studies investigating two different BET proteins in two different cell types suggest that in addition to recognizing acetylated histones, bromodomains may also interact broadly with RNAs. In both studies, depletion of noncoding RNAs inhibited BET protein occupancy and activity at specific genes. Future investigation will be required to elucidate how RNAs may affect recognition of acetylated histones.

RNAs can interact with proteins to form condensates[26,27,50]. The interaction between *DIGIT* and BRD3 expands our understanding of the involvement of lncRNAs in condensates[51,52] and demonstrates a role for lncRNAs in transcriptional phase-separated condensates. BRD4 forms phase-separated condensates in association with Mediator to regulate gene expression[17], and BRD2, BRD3 and BRD4 form distinct phase-separated condensates during endoderm differentiation. *DIGIT* promotes the formation of BRD3 condensates in

endoderm differentiation. BRD3 also interacts with other RNA transcripts in addition to *DIGIT*, and we anticipate future studies will identify other RNA partners that preferentially interact with individual BET proteins to promote the formation of condensates in specific cell types.

Our findings indicate that the interactions between BET proteins and lncRNAs help specify gene targets. This interaction is not limited to polyA RNAs, as eRNAs can also bind BET proteins[49]. Interactions with specific RNA transcripts may control the regulation of subsets of genes targeted by BET proteins, and changes in RNA species between different cell types may add an additional layer of cell-type-specific control to BET proteins.
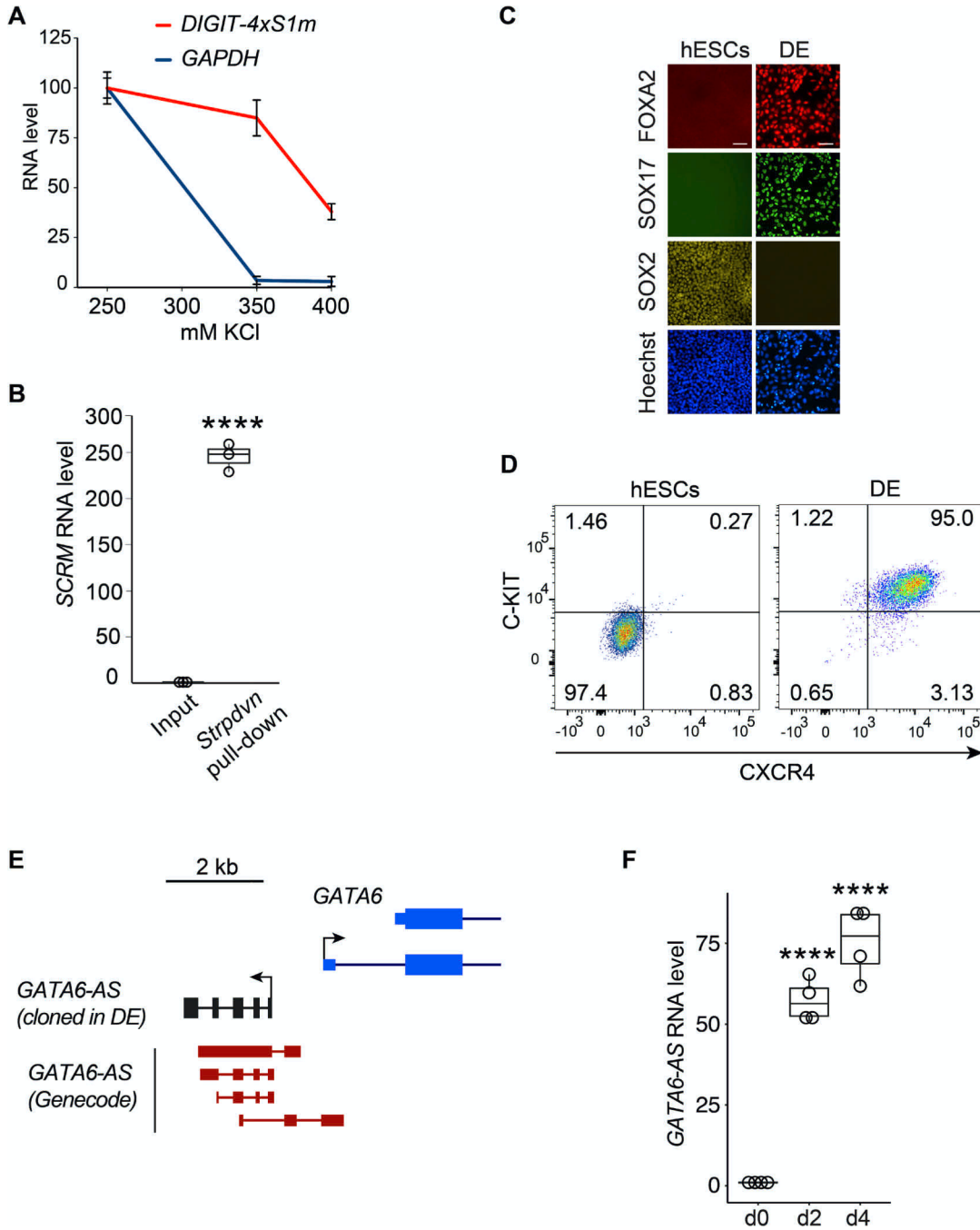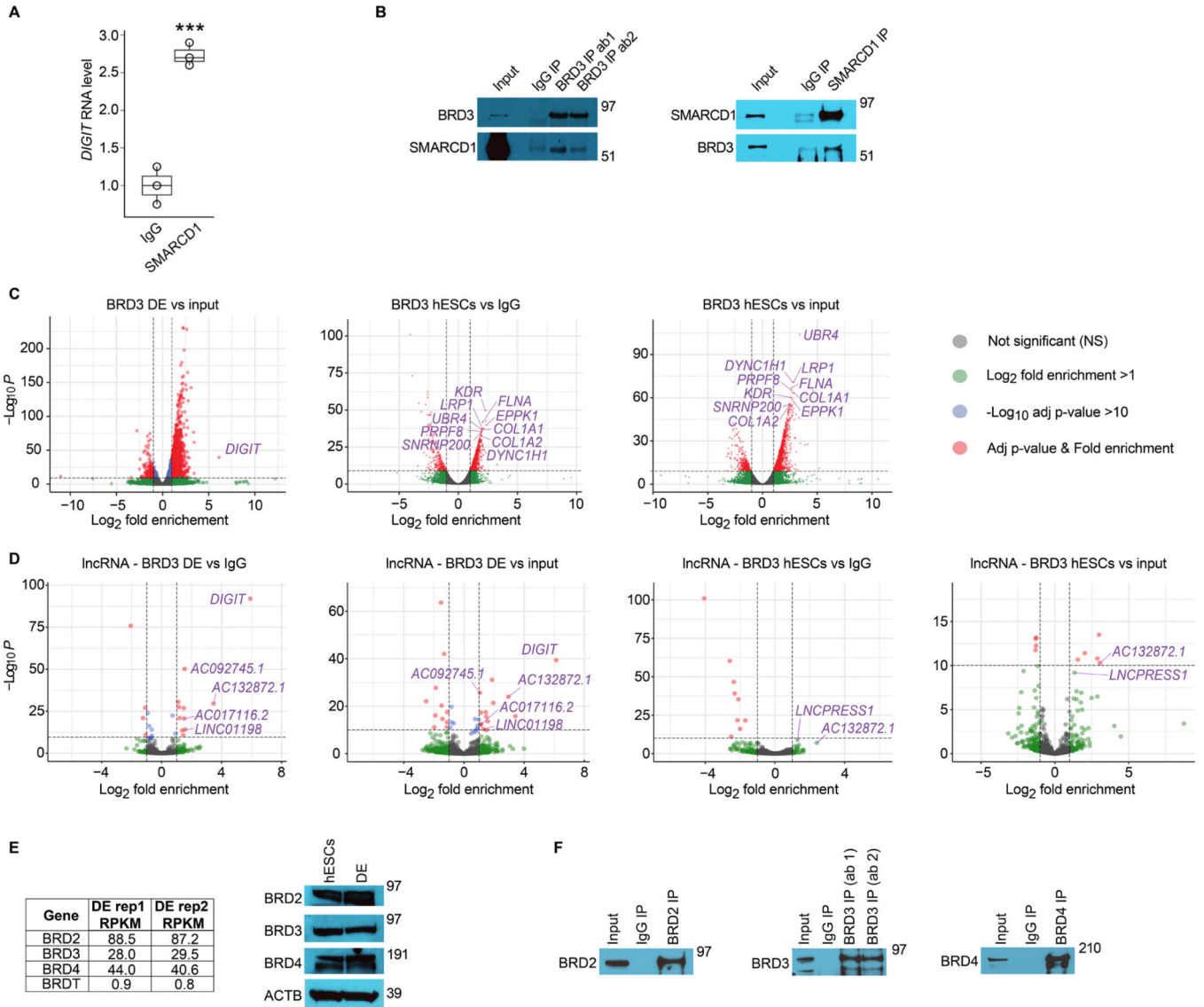
Extended Data

Extended Data Fig. 1. Optimization of RNA pull-down, endoderm differentiation, and evaluation of *GATA6-AS* in endoderm.
(**A**) Recovery of *DIGIT-4S1m* versus endogenous *GAPDH* mRNA with increasing concentrations of KCl. RNA recovered with 250 mM KCl is set to 100 for each RNA species. Error bars represent the standard deviation of n=3 independent experiments. (**B**) Enrichment of *SCRM-4xS1m* after streptavidin pull-down as quantified by qRT-PCR. The transcript level in input was set to 1.0. RNA levels are normalized to *GAPDH*. ****

indicates p <0.0001 (Student's t-test, n=3 independent experiments). Box plots show the first and third quartiles, median (horizontal line), and minimum and maximum values (whiskers). **(C)** Immunostaining shows the differentiation of hESCs to definitive endoderm (DE). FOXA2 (red) and SOX17 (green) are used as markers of definitive endoderm. SOX2 (yellow) is used as a marker of pluripotency. Hoechst staining (blue) marks nuclei. Scale bar represents 100 μm. This experiment was performed twice with similar results. **(D)** Flow cytometry plots show the population of cells that are CXCR4 and c-KIT double-positive in hESCs and DE cells generated using the high-efficiency DE differentiation protocol[1]. This experiment was performed three times with similar results. **(E)** The diagram shows the gene encoding lncRNA *GATA6-AS*, which is divergently transcribed from the gene encoding GATA6. Annotated *GATA6-AS* transcripts are shown in red and the transcript cloned in DE cells is shown in black. **(F)** qRT-PCR shows levels of *GATA6-AS* in hESCs and on the indicated days of endoderm differentiation. Box plots show the first and third quartiles, median (horizontal line), and minimum and maximum values (whiskers). **** indicates p <0.0001 compared to day 0 (One-way ANOVA, n=4 independent experiments). Statistical source data are provided in Source data extended data Fig. 1.

Extended Data Figure 2. RIP-seq, expression of BET proteins in endoderm, and interactions with SMARCD1.

(A) RIP shows the levels of *DIGIT* following SMARCD1 and IgG immunoprecipitation. *** indicates p<0.001 n=3 independent experiments. Box plots show the first and third quartiles, median (horizontal line), and minimum and maximum values (whiskers). **(B)** Co-immunoprecipitation followed by immunoblotting shows the interaction of BRD3 and SMARCD1. This experiment was performed twice with similar results. **(C)** Volcano plots show transcripts enriched with BRD3 RIP. Transcripts from BRD3 RIP were normalized to IgG RIP for endoderm cells (DE, Figure 1G) and normalized to total nuclear RNA (input), left. BRD3 RIP normalized to IgG (center) and input (right) are shown for hESCs. The 10 most enriched transcripts in common between IgG and input for hESCs are labeled on the volcano plots. Points are colored to indicate different thresholds as labeled on the far right. RIP-seq was performed in two independent samples and pooled for analysis. **(D)** Volcano plots show lncRNA transcripts enriched with BRD3 RIP when normalized to IgG or input in

DE (left) and hESCs (right). lncRNA transcripts in common between IgG and input controls are labeled (purple). Points are shaded to indicate different thresholds as in (C). RIP-seq was performed in two independent samples and pooled for analysis.**(E)** The table (left) shows normalized expression values (RPKM) in endoderm differentiation[2]. Immunoblot (right) shows the protein levels of BET proteins with differentiation. Beta-Actin (ACTB) is used as a loading control. This experiment was performed twice with similar results. **(F)** Immunoprecipitation was performed using antibodies specific to each BET protein. IgG serves as a control. This experiment was performed twice with similar results. Unprocessed blots and statistical source data are provided in Source data extended data Fig. 2.
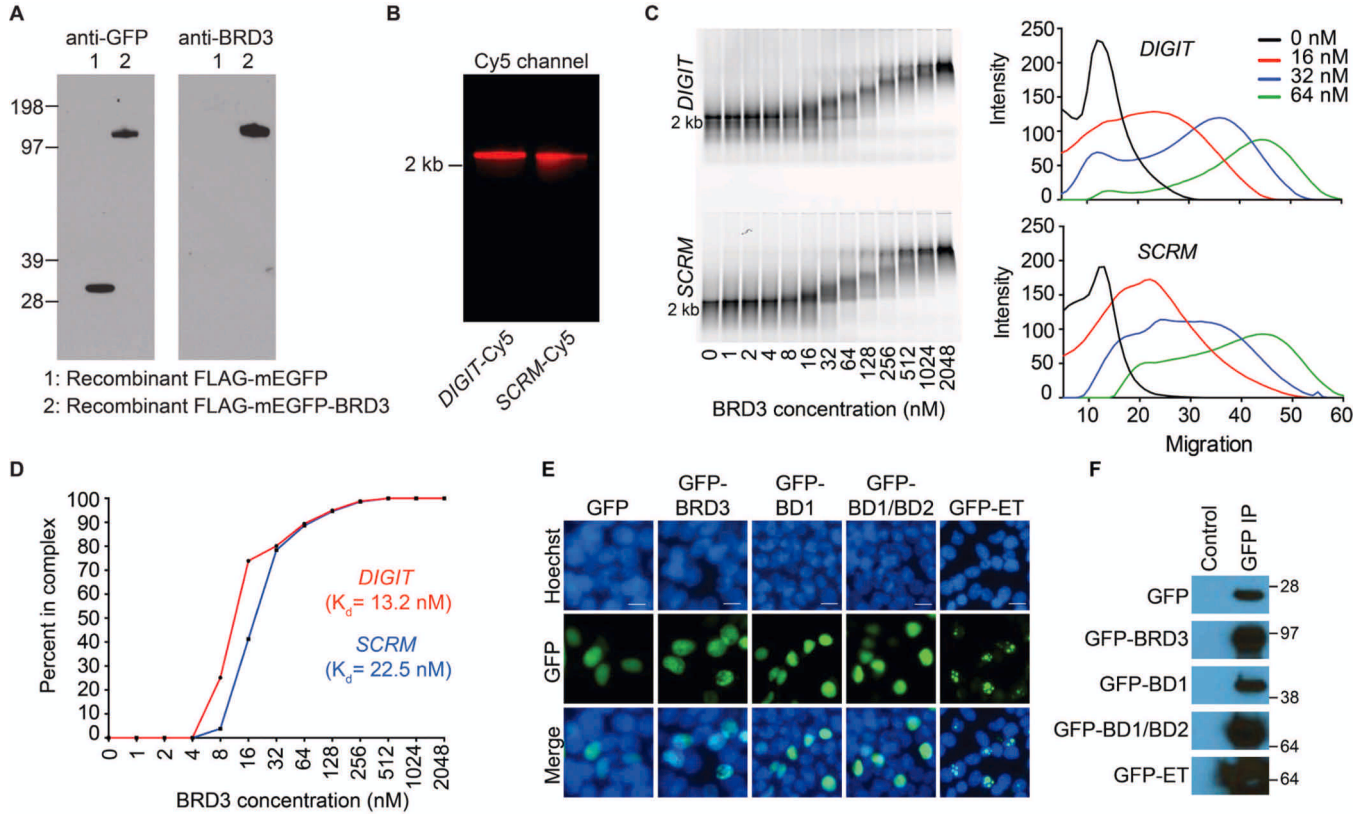
Extended Data Figure 3. Generation of recombinant BRD3 and GFP, production of Cy-5 labeled RNAs, EMSA replicate, localization of BRD3 domains, and immunoprecipitation of BRD3 domains.

(A) Immunoblot was performed to detect recombinant FLAG-mEGFP-BRD3 (long isoform) and FLAG-mEGFP using an anti-GFP antibody (left) and an anti-BRD3 antibody (right). **(B)** Fluorescent detection of the Cy5-labeled *DIGIT* and *SCRM* on a 1% bleach-agarose gel. Experiments in A and B were performed twice with similar results. **(C)** Replicate electrophoretic mobility shift assay (EMSA) of *in vitro* transcribed *DIGIT* (left, top) and *SCRM* (left, bottom), which are labeled with Cy5 and incubated with recombinant BRD3. Migration was visualized on the right by quantifying the signal for *DIGIT* (top) or *SCRM* (bottom) across the gel. Migration of 0 on the x-axis was defined by the peak of *DIGIT* and *SCRM* with 0 nM BRD3 protein, and migration of 100 was defined by the peak of *DIGIT* and *SCRM* with 2048 nM BRD3 protein. This experiment shows a second replicate of

Figure 2C. **(D)** The dissociation constants (Kd) were calculated for (C). **(E)** Fluorescence microscopy shows the nuclear localization of ectopically expressed GFP, GFP fused to full-length BRD3, and GFP fused to the indicated bromodomains (BD) or extra terminal (ET) domains of BRD3 in HEK 293 cells. Scale bar represents 20 μm. This experiment was performed twice with similar results. **(F)** Immunoprecipitation followed by immunoblotting using an antibody against GFP shows the precipitation of the proteins described in (E). This experiment was performed twice with similar results. Unprocessed blots are provided in Source data extended data Fig. 3.
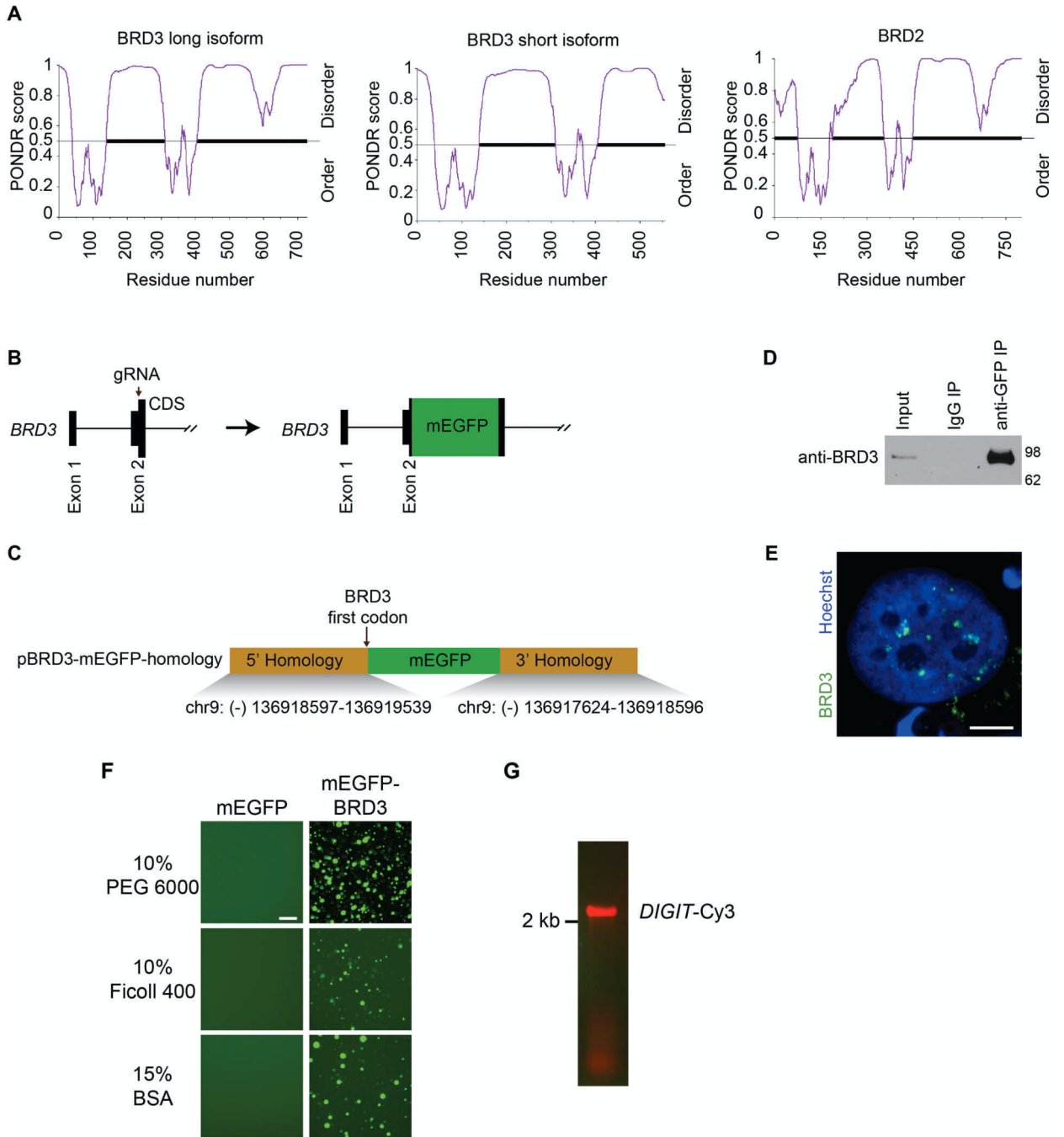
Extended Data Figure 4. Prediction of ordered/disordered protein structures, strategy for tagging endogenous BRD3 with mEGFP, formation of BRD3 puncta in hESCs, and in vitro droplet formation.

(A) PONDR VSL2 plots showing the ordered and disordered regions of the long (left) and short (middle) isoforms of BRD3, and BRD2 (right). **(B)** Creation of mEGFP-BRD3 fusion protein. The cDNA encoding mEGFP was inserted at the N-terminus of *BRD3*. This terminus is shared by the long and short isoforms of BRD3. The site targeted by gRNA is indicated with an arrow. The start of the coding sequence (CDS) is indicated, and the mEGFP cDNA is inserted in frame after the start codon. **(C)** Design of the homology vector
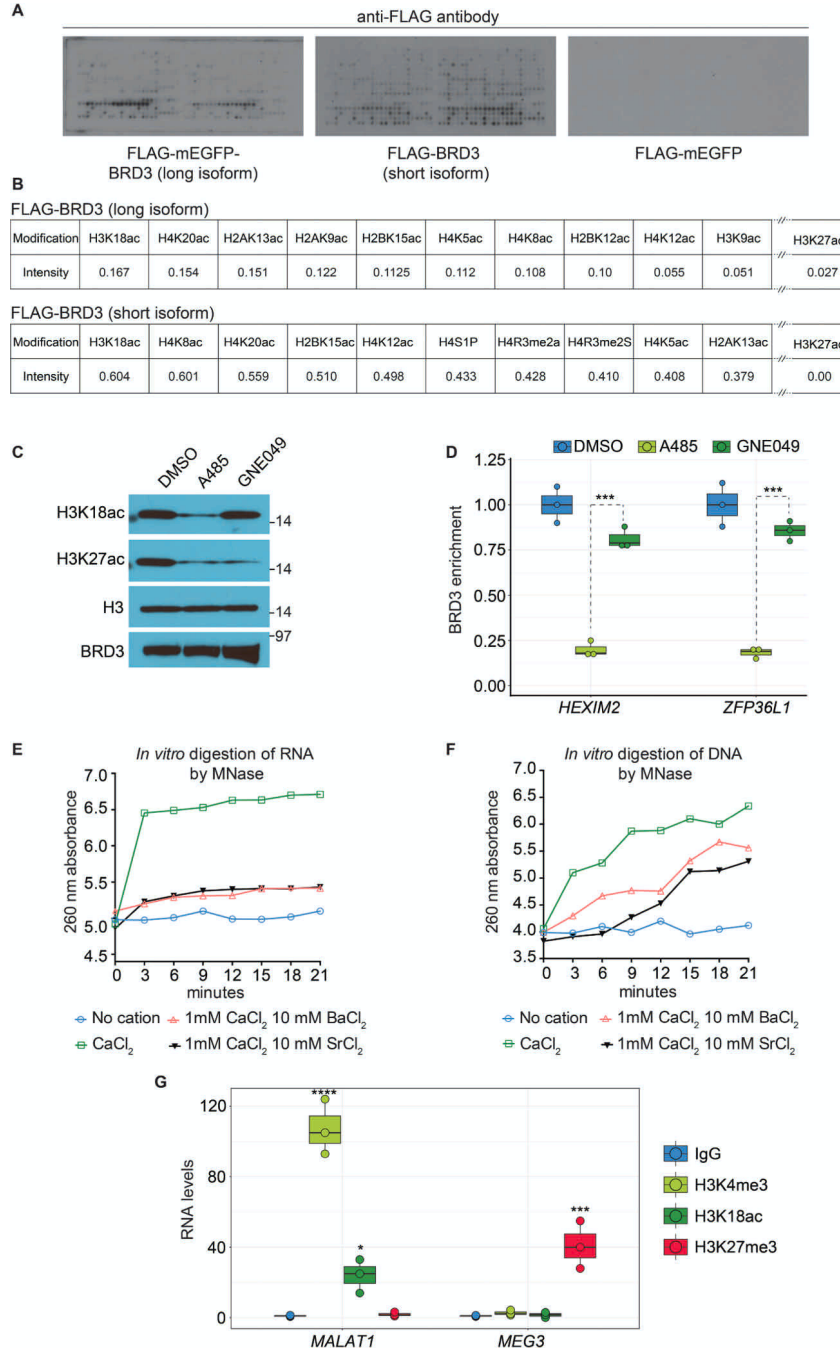
for the insertion of mEGFP. The genomic locations of homology arms are indicated. Arrow indicates that mEGFP was inserted after the start codon for *BRD3*. **(D)** Immunoblot using anti-BRD3 antibody confirms the generation of mEGFP-BRD3 fused protein. hESCs were lysed and IP was performed using an IgG isotype control and an antibody recognizing GFP. Total cell lysates (input) and the IPs were then probed with an anti-BRD3 antibody. This experiment was performed twice with similar results. **(E)** Immunofluorescence of an hESC showing BRD3 puncta (green) in the nucleus (blue). Scale bar represents 10 μm. This experiment was performed twice with similar results. **(F)** Droplet assay shows the formation of mEGFP-BRD3 droplets in the presence of three different molecular crowding agents. Scale bar represents 2 μm. This experiment was performed three times with similar results. **(G)** Fluorescent detection of the Cy3-labeled *DIGIT* and *SCRM* on a 1% bleach-agarose gel. This experiment was performed twice with similar results.
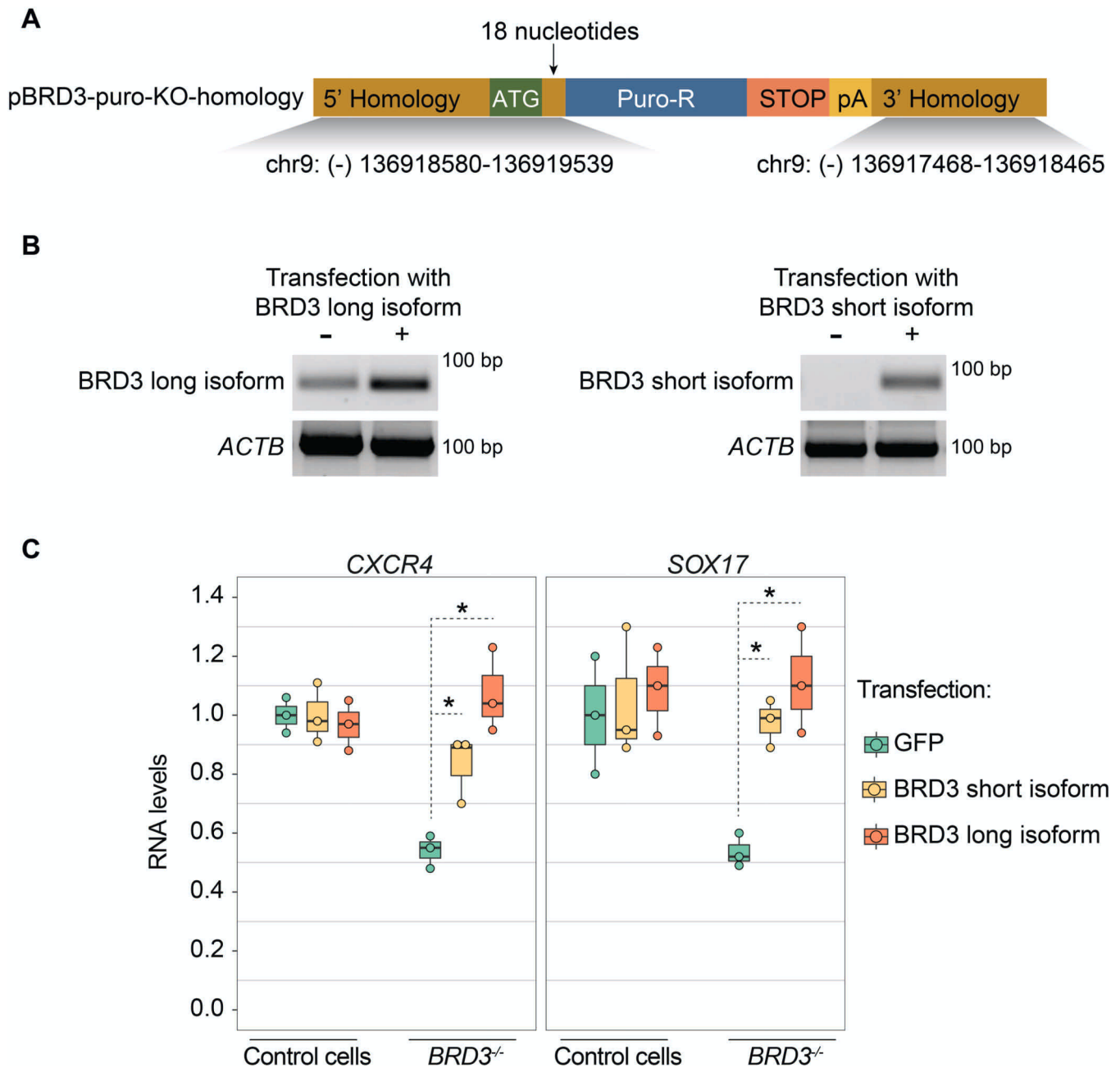
Extended Data Figure 5. Homology construct for targeting BRD3, and analysis of long and short isoforms of BRD3.
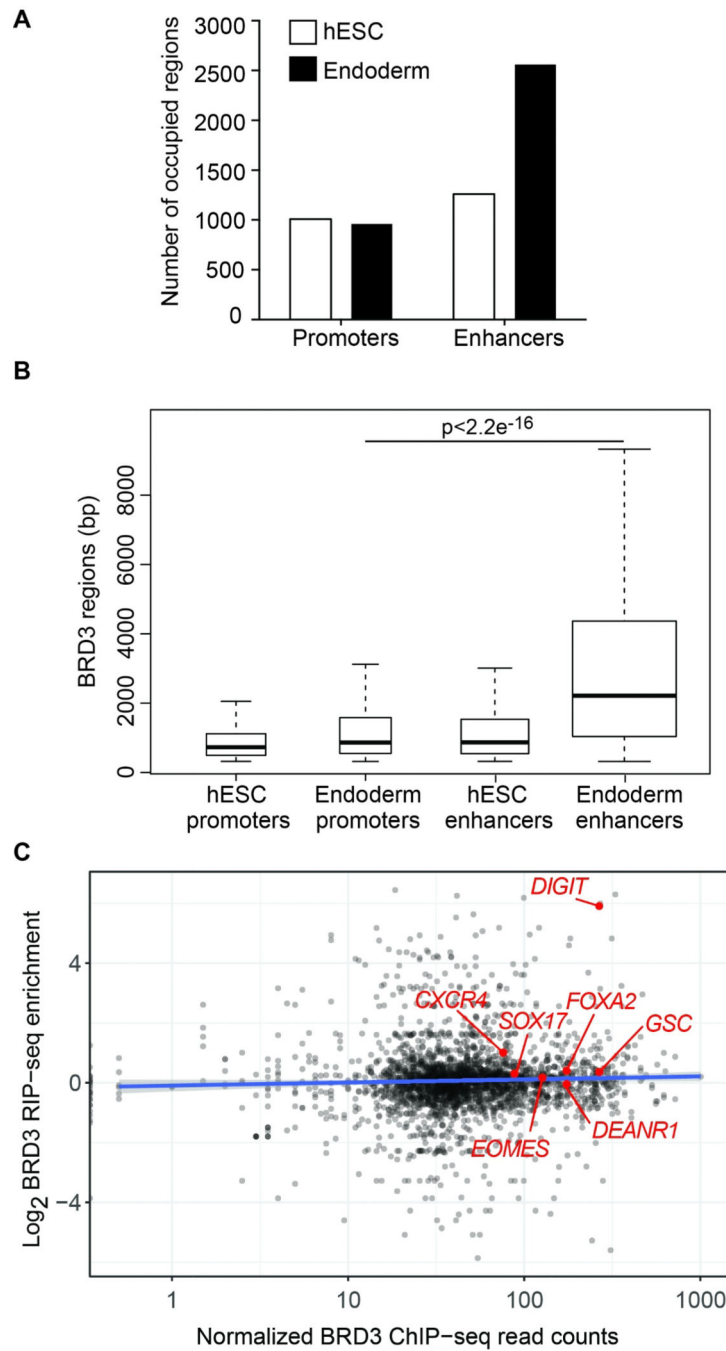(**A**) Map of the homology construct for insertion of a puromycin resistance cassette and a stop codon cassette downstream of the sixth codon of the gene encoding BRD3. (**B**) hESCs were differentiated towards DE for three days prior to qRT-PCR. Primers that uniquely recognize either the long (left) or short (right) isoforms of BRD3 were used for amplification. Cells were also transfected with plasmids expressing the long (left) and short (right) isoforms of BRD3 as positive (+) controls for the primers. The long isoform of BRD3 is detected with DE differentiation while the short isoform is not detected. *ACTB* was used as a control. This experiment was performed twice with similar results. (**C**) Wildtype and

BRD3⁻/⁻ hESCs were transfected with plasmids expressing GFP (green), the short isoform of BRD3 (yellow), and the long isoform of BRD3 (orange). Expression of *CXCR4* and *SOX17* was quantified by qRT-PCR after three days of DE differentiation. Ectopic expression of both the long and short isoform of BRD3 rescued expression of *CXCR4* and *SOX17.* * indicates p<0.05 (n=3 independent experiments). Box plots show the first and third quartiles, median (horizontal line), and minimum and maximum values (whiskers). Statistical source data are provided in Source data extended data Fig. 5

A anti-FLAG antibody

FLAG-mEGFP-BRD3 (long isoform) | FLAG-BRD3 (short isoform) | FLAG-mEGFP

B

FLAG-BRD3 (long isoform)

Modification	H3K18ac	H4K20ac	H2AK13ac	H2AK9ac	H2BK15ac	H4K5ac	H4K8ac	H2BK12ac	H4K12ac	H3K9ac	H3K27ac
Intensity	0.167	0.154	0.151	0.122	0.1125	0.112	0.108	0.10	0.055	0.051	0.027

FLAG-BRD3 (short isoform)

Modification	H3K18ac	H4K8ac	H4K20ac	H2BK15ac	H4K12ac	H4S1P	H4R3me2a	H4R3me2S	H4K5ac	H2AK13ac	H3K27ac
Intensity	0.604	0.601	0.559	0.510	0.498	0.433	0.428	0.410	0.408	0.379	0.00

Extended Data Figure 6. Binding of BRD3 to modified histones, effects of inhibition of P300 on the enrichment of BRD3, the activity of MNase in presence of Ba^{+2} and Sr^{+2} cations, and enrichment of lncRNAs in specific histone modifications.

(A) Peptide arrays show the binding of recombinant BRD3 to histone modifications. **(B)** Spot intensity of BRD3 (long and short isoforms, top and bottom respectively) binding to the top ten histone modifications as quantified by image processing software (see Materials and Methods). **(C)** Immunoblots to detect the levels of acetylation on H3K18 and H3K27, as well as levels of BRD3 and total H3 in hESCs treated with DMSO, A485, or GNE049. This experiment was performed twice with similar results. **(D)** CUT&RUN followed by qPCR shows the enrichment of BRD3 at the *HEXIM2* and *ZFP36L1* loci in hESCs. Box plots show the first and third quartiles, median (horizontal line), and minimum and maximum values (whiskers). *** indicates p <0.001 (Student's t-test, n=3 independent experiments). **(E)** RNase activity of MNase in the presence of Ba^{2+} and Sr^{2+} cations. This experiment was performed twice with similar results. **(F)** DNase activity of MNase in the presence of Ba^{2+} and Sr^{2+} cations. This experiment was performed twice with similar results. **(G)** CUT&RUNER followed by qPCR shows the enrichment of *MALAT1* and *MEG3* transcripts in IgG control, markers of gene activation (H3K4me3 and H3K18ac) and repression (H3K27me3). Box plots show the first and third quartiles, median (horizontal line), and minimum and maximum values (whiskers). * indicates p < 0.05, *** indicates p <0.001, and **** indicates p < 0.0001 compared to IgG (Student's t-test, n=3 independent experiments). Statistical source data are provided in Source data extended data Fig. 6.

A The number of BRD3 regions (y-axis) that contain promoters and enhancers are shown for hESCs (white) and endoderm cells (black). BRD3 regions are defined as containing promoters if the region is located within 2kb of a transcription start site (TSS). BRD3 regions are defined as containing enhancers if the region overlaps with enhancers defined by H3K27ac. Regions that contain both promoters and enhancers are counted in both categories. In Figure 7A, BRD3 regions are first evaluated for association with promoters.

Extended Data Figure 7. BRD3 occupies endoderm genes and enhancers and interaction between BRD3 and *DIGIT* is not dependent on location of transcription.

Regions that are not associated with promoters are then evaluated for association with enhancers (See Supplementary Methods). Data from two independent BRD3 ChIPs were pooled for analysis of hESCs and DE. **(B)** Box plots show the length of regions occupied by BRD3 for the categories described in (A). The bold horizontal line represents the median for each box plot. The lower edge of the box represents the first quartile (Q1) and the upper edge of the box represents the third quartile (Q3). The lower whiskers represent Q1–1.5*(Q3-Q1) and the upper whisker represents Q3+1.5*(Q3-Q1). The width of each box is proportional to the number of BRD3 regions in each category. Data from two independent BRD3 ChIPs were pooled for analysis of hESCs and DE. The width of each box is proportional to the number of BRD3 regions in each category. Data from two independent BRD3 ChIPs were pooled for analysis of hESCs and DE. **(C)** Transcript enrichment from BRD3 RIP in DE vs IgG control (Figure 1G, y-axis) is shown for each gene occupied by BRD3 in DE (x-axis). Endoderm genes are labeled in red. Data from two independent BRD3 ChIPs and two independent BRD3 RIPs were pooled for analysis.
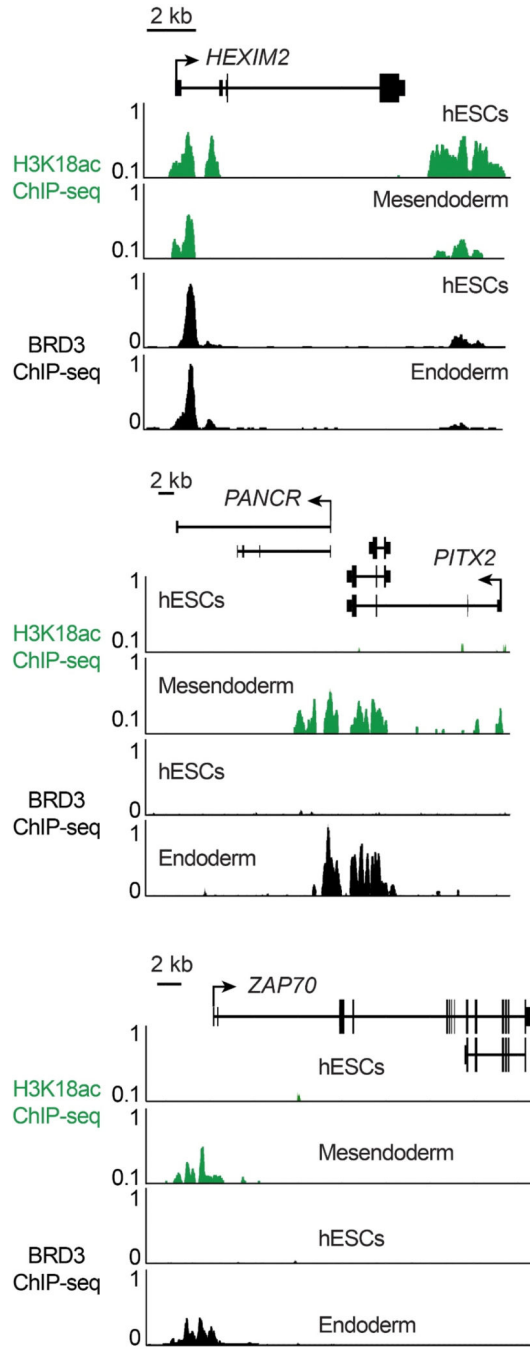
Extended Data Figure 8. BRD3 occupancy at genes not regulated by *DIGIT*.
ChIP-seq data shows H3K18ac (top, green) and BRD3 occupancy (bottom, black) at
HEXIM2, PITX2/PANCR and *ZAP70* in hESCs and endoderm/mesendoderm cells. BRD3
occupies *HEXIM2* in hESCs and mesendoderm/endoderm. BRD3 occupies *PITX2/PANCR*
and *ZAP70* in mesendoderm/endoderm but not in hESCs. Data from two independent BRD3
ChIPs were pooled for analysis. H3K18ac was analyzed from GSE16256.

Supplementary Material

Refer to Web version on PubMed Central for supplementary material.

Acknowledgments

References

1. Flynn RA & Chang HY Long noncoding RNAs in cell-fate programming and reprogramming. Cell Stem Cell 14, 752–761 (2014). [PubMed: 24905165]

2. Perry RB-T & Ulitsky I The functions of long noncoding RNAs in development and stem cells. Development 143, 3882–3894 (2016). [PubMed: 27803057]

3. Jiang W, Liu Y, Liu R, Zhang K & Zhang Y The lncRNA DEANR1 Facilitates Human Endoderm Differentiation by Activating FOXA2 Expression. Cell Rep. 11, 137–148 (2015). [PubMed: 25843708]

4. Daneshvar K et al. DIGIT Is a Conserved Long Noncoding RNA that Regulates GSC Expression to Control Definitive Endoderm Differentiation of Embryonic Stem Cells. Cell Rep. 17, 1–13 (2016). [PubMed: 27681415]

5. Bell CC et al. The Evx1/Evx1as gene locus regulates anterior-posterior patterning during gastrulation. Sci. Rep 6, 26657 (2016). [PubMed: 27226347]

6. Luo S et al. Divergent lncRNAs Regulate Gene Expression and Lineage Differentiation in Pluripotent Cells. Cell Stem Cell 1–16 (2016).

7. Kanno T et al. Selective recognition of acetylated histones by bromodomain proteins visualized in living cells. Mol. Cell 13, 33–43 (2004). [PubMed: 14731392]

8. Filippakopoulos P et al. Histone recognition and large-scale structural analysis of the human bromodomain family. Cell 149, 214–231 (2012). [PubMed: 22464331]

9. Paillisson A et al. Bromodomain testis-specific protein is expressed in mouse oocyte and evolves faster than its ubiquitously expressed paralogs BRD2, –3, and –4. Genomics 89, 215–223 (2007). [PubMed: 17049203]

10. Wai DCC et al. The BRD3 ET domain recognizes a short peptide motif through a mechanism that is conserved across chromatin remodelers and transcriptional regulators. J. Biol. Chem 293, 7160–7175 (2018). [PubMed: 29567837]

11. Deeney JT, Belkina AC, Shirihai OS, Corkey BE & Denis GV BET Bromodomain Proteins Brd2, Brd3 and Brd4 Selectively Regulate Metabolic Pathways in the Pancreatic β-Cell. PLoS One 11, e0151329 (2016). [PubMed: 27008626]

12. Jang MK et al. The Bromodomain Protein Brd4 Is a Positive Regulatory Component of P-TEFb and Stimulates RNA Polymerase II-Dependent Transcription. Mol. Cell 19, 523–534 (2005). [PubMed: 16109376]

13. Houzelstein D et al. Growth and early postimplantation defects in mice deficient for the bromodomain-containing protein Brd4. Mol. Cell. Biol 22, 3794–3802 (2002). [PubMed: 11997514]

14. Shang E, Wang X, Wen D, Greenberg DA & Wolgemuth DJ Double bromodomain-containing gene Brd2 is essential for embryonic development in mouse. Dev. Dyn 238, 908–917 (2009). [PubMed: 19301389]

15. Di Micco R et al. Control of embryonic stem cell identity by BRD4-dependent transcriptional elongation of super-enhancer-associated pluripotency genes. Cell Rep. 9, 234–247 (2014). [PubMed: 25263550]

16. Fernandez-Alonso R et al. Brd4-Brd2 isoform switching coordinates pluripotent exit and Smad2-dependent lineage specification. EMBO Rep. 18, 1108–1122 (2017). [PubMed: 28588073]

17. Sabari BR et al. Coactivator condensation at super-enhancers links phase separation and gene control. Science 361, (2018).

18. Leppek K & Stoecklin G An optimized streptavidin-binding RNA aptamer for purification of ribonucleoprotein complexes identifies novel ARE-binding proteins. Nucleic Acids Res. 42, e13 (2014). [PubMed: 24157833]

19. Srisawat C & Engelke DR Streptavidin aptamers: affinity tags for the study of RNAs and ribonucleoproteins. RNA 7, 632–641 (2001). [PubMed: 11345441]

20. Neumann P et al. The lncRNA GATA6-AS epigenetically regulates endothelial gene expression via interaction with LOXL2. Nat. Commun 9, 237 (2018). [PubMed: 29339785]

21. Oh J et al. BAF60a interacts with p53 to recruit the SWI/SNF complex. J. Biol. Chem 283, 11924–11934 (2008). [PubMed: 18303029]

22. Alajem A et al. Differential association of chromatin proteins identifies BAF60a/SMARCD1 as a regulator of embryonic stem cell differentiation. Cell Rep. 10, 2019–2031 (2015). [PubMed: 25818293]

23. Maori E et al. A Secreted RNA Binding Protein Forms RNA-Stabilizing Granules in the Honeybee Royal Jelly. Mol. Cell 74, 598–608.e6 (2019). [PubMed: 31051140]

24. Queiroz RML et al. Comprehensive identification of RNA-protein interactions in any organism using orthogonal organic phase separation (OOPS). Nat. Biotechnol 37, 169–178 (2019). [PubMed: 30607034]

25. Kato M et al. Cell-free formation of RNA granules: low complexity sequence domains form dynamic fibers within hydrogels. Cell 149, 753–767 (2012). [PubMed: 22579281]

26. Li P et al. Phase transitions in the assembly of multivalent signalling proteins. Nature 483, 336–340 (2012). [PubMed: 22398450]

27. Lin Y, Protter DSW, Rosen MK & Parker R Formation and Maturation of Phase-Separated Liquid Droplets by RNA-Binding Proteins. Mol. Cell 60, 208–219 (2015). [PubMed: 26412307]

28. Lu H et al. Phase-separation mechanism for C-terminal hyperphosphorylation of RNA polymerase II. Nature 558, 318–323 (2018). [PubMed: 29849146]

29. Boija A et al. Transcription Factors Activate Genes through the Phase-Separation Capacity of Their Activation Domains. Cell 175, 1842–1855.e16 (2018). [PubMed: 30449618]

30. Banani SF, Lee HO, Hyman AA & Rosen MK Biomolecular condensates: organizers of cellular biochemistry. Nat. Rev. Mol. Cell Biol 18, 285–298 (2017). [PubMed: 28225081]

31. Kowarz E, Löscher D & Marschalek R Optimized Sleeping Beauty transposons rapidly generate stable transgenic cell lines. Biotechnol. J 10, 647–653 (2015). [PubMed: 25650551]

32. Deglincerti A, Etoc F, Ozair MZ & Brivanlou AH Self-Organization of Spatial Patterning in Human Embryonic Stem Cells. Curr. Top. Dev. Biol 116, 99–113 (2016). [PubMed: 26970615]

33. Warmflash A, Sorre B, Etoc F, Siggia ED & Brivanlou AH A method to recapitulate early embryonic spatial patterning in human embryonic stem cells. Nat. Methods 11, 847–854 (2014). [PubMed: 24973948]

34. Jin Q et al. Distinct roles of GCN5/PCAF-mediated H3K9ac and CBP/p300-mediated H3K18/27ac in nuclear receptor transactivation. EMBO J. 30, 249–262 (2011). [PubMed: 21131905]

35. Lasko LM et al. Discovery of a selective catalytic p300/CBP inhibitor that targets lineage-specific tumours. Nature 550, 128–132 (2017). [PubMed: 28953875]

36. Raisner R et al. Enhancer Activity Requires CBP/P300 Bromodomain-Dependent Histone H3K27 Acetylation. Cell Rep. 24, 1722–1729 (2018). [PubMed: 30110629]

37. Tada S et al. Characterization of mesendoderm: a diverging point of the definitive endoderm and mesoderm in embryonic stem cell differentiation culture. Development 132, 4363–4374 (2005). [PubMed: 16141227]

38. Vallier L et al. Early cell fate decisions of human embryonic stem cells and mouse epiblast stem cells are controlled by the same signalling pathways. PLoS One 4, e6082 (2009). [PubMed: 19564924]

39. Skene PJ & Henikoff S An efficient targeted nuclease strategy for high-resolution mapping of DNA binding sites. Elife 6, (2017).

40. Cuatrecasas P, Fuchs S & Anfinsen CB Catalytic properties and specificity of the extracellular nuclease of Staphylococcus aureus. J. Biol. Chem 242, 1541–1547 (1967). [PubMed: 4290246]

41. West JA et al. The Long Noncoding RNAs NEAT1 and MALAT1 Bind Active Chromatin Sites. Mol. Cell 55, 791–802 (2014). [PubMed: 25155612]

42. Mondal T et al. MEG3 long noncoding RNA regulates the TGF-β pathway genes through formation of RNA–DNA triplex structures. Nature Communications vol. 6 (2015).

43. Dixon JR et al. Chromatin architecture reorganization during stem cell differentiation. Nature 518, 331–336 (2015). [PubMed: 25693564]

44. Kopp F & Mendell JT Functional Classification and Experimental Dissection of Long Noncoding RNAs. Cell 172, 393–407 (2018). [PubMed: 29373828]

45. Xi Q et al. A poised chromatin platform for TGF-β access to master regulators. Cell 147, 1511–1524 (2011). [PubMed: 22196728]

46. Luo M et al. H3K18ac Primes Mesendodermal Differentiation upon Nodal Signaling. Stem Cell Reports 13, 642–656 (2019). [PubMed: 31564646]

47. Pouponnot C, Jayaraman L & Massagué J Physical and functional interaction of SMADs and p300/CBP. J. Biol. Chem 273, 22865–22868 (1998). [PubMed: 9722503]

48. Janknecht R, Wells NJ & Hunter T TGF-beta-stimulated cooperation of smad proteins with the coactivators CBP/p300. Genes Dev. 12, 2114–2119 (1998). [PubMed: 9679056]

49. Rahnamoun H et al. RNAs interact with BRD4 to promote enhanced chromatin engagement and transcription activation. Nat. Struct. Mol. Biol 25, 687–697 (2018). [PubMed: 30076409]

50. Molliex A et al. Phase separation by low complexity domains promotes stress granule assembly and drives pathological fibrillization. Cell 163, 123–133 (2015). [PubMed: 26406374]

51. Yamazaki T et al. Functional Domains of NEAT1 Architectural lncRNA Induce Paraspeckle Assembly through Phase Separation. Mol. Cell 70, 1038–1053.e7 (2018). [PubMed: 29932899]

52. Hutchinson JN et al. A screen for nuclear transcripts identifies two linked noncoding RNAs associated with SC35 splicing domains. BMC Genomics 8, 39 (2007). [PubMed: 17270048]

53. Loh KM et al. Efficient endoderm induction from human pluripotent stem cells by logically directing signals controlling lineage bifurcations. Cell Stem Cell 14, 237–252 (2014). [PubMed: 24412311]

54. Deglincerti A et al. Self-organization of human embryonic stem cells on micropatterns. Nat. Protoc 11, 2223–2232 (2016). [PubMed: 27735934]

55. Mellacheruvu D et al. The CRAPome: a contaminant repository for affinity purification-mass spectrometry data. Nat. Methods 10, 730–736 (2013). [PubMed: 23921808]

56. Skene PJ, Henikoff JG & Henikoff S Targeted in situ genome-wide profiling with high efficiency for low cell numbers. Nat. Protoc 13, 1006–1019 (2018). [PubMed: 29651053]

57. Putnam FW & Neurath H The Precipitation of Proteins by Synthetic Detergents 1a. J. Am. Chem. Soc 66, 692–697 (1944).

58. Rinn JL et al. Functional demarcation of active and silent chromatin domains in human HOX loci by noncoding RNAs. Cell 129, 1311–1323 (2007). [PubMed: 17604720]

59. Chicaybam L, Sodre AL, Curzio BA & Bonamino MH An Efficient Low Cost Method for Gene Transfer to T Lymphocytes. PLoS One 8, e60298 (2013). [PubMed: 23555950]

60. Grau DJ et al. Compaction of chromatin by diverse Polycomb group proteins requires localized regions of high charge. Genes Dev. 25, 2210–2221 (2011). [PubMed: 22012622]

61. Abmayr SM, Yao T, Parmely T & Workman JL Preparation of nuclear and cytoplasmic extracts from mammalian cells. Curr. Protoc. Mol. Biol Chapter 12, Unit 12.1 (2006).

62. Saltzman AL, Soo MW, Aram R & Lee JT Multiple Histone Methyl-Lysine Readers Ensure Robust Development and Germline Immortality in. Genetics (2018) doi:10.1534/genetics.118.301518.

63. Aranda PS, LaJoie DM & Jorcyk CL Bleach gel: a simple agarose gel for analyzing RNA quality. Electrophoresis 33, 366–369 (2012). [PubMed: 22222980]

64. Langmead B & Salzberg SL Fast gapped-read alignment with Bowtie 2. Nat. Methods 9, 357–359 (2012). [PubMed: 22388286]

65. Li H et al. The Sequence Alignment/Map format and SAMtools. Bioinformatics 25, 2078–2079 (2009). [PubMed: 19505943]

66. Zhang Y et al. Model-based analysis of ChIP-Seq (MACS). Genome Biol. 9, R137 (2008). [PubMed: 18798982]

67. Creyghton MP et al. Histone H3K27ac separates active from poised enhancers and predicts developmental state. Proc. Natl. Acad. Sci. U. S. A 107, 21931–21936 (2010). [PubMed: 21106759]

68. Rada-Iglesias A et al. A unique chromatin signature uncovers early developmental enhancers in humans. Nature 470, 279–283 (2011). [PubMed: 21160473]

69. Kent WJ, Zweig AS, Barber G, Hinrichs AS & Karolchik D BigWig and BigBed: enabling browsing of large distributed datasets. Bioinformatics 26, 2204–2207 (2010). [PubMed: 20639541]

70. Ramírez F et al. deepTools2: a next generation web server for deep-sequencing data analysis. Nucleic Acids Res. 44, W160–5 (2016). [PubMed: 27079975]

71. Anders S, Pyl PT & Huber W HTSeq--a Python framework to work with high-throughput sequencing data. Bioinformatics 31, 166–169 (2015). [PubMed: 25260700]

72. Ito T, Ikehara T, Nakagawa T, Kraus WL & Muramatsu M p300-mediated acetylation facilitates the transfer of histone H2A-H2B dimers from nucleosomes to a histone chaperone. Genes Dev. 14, 1899–1907 (2000). [PubMed: 10921904]
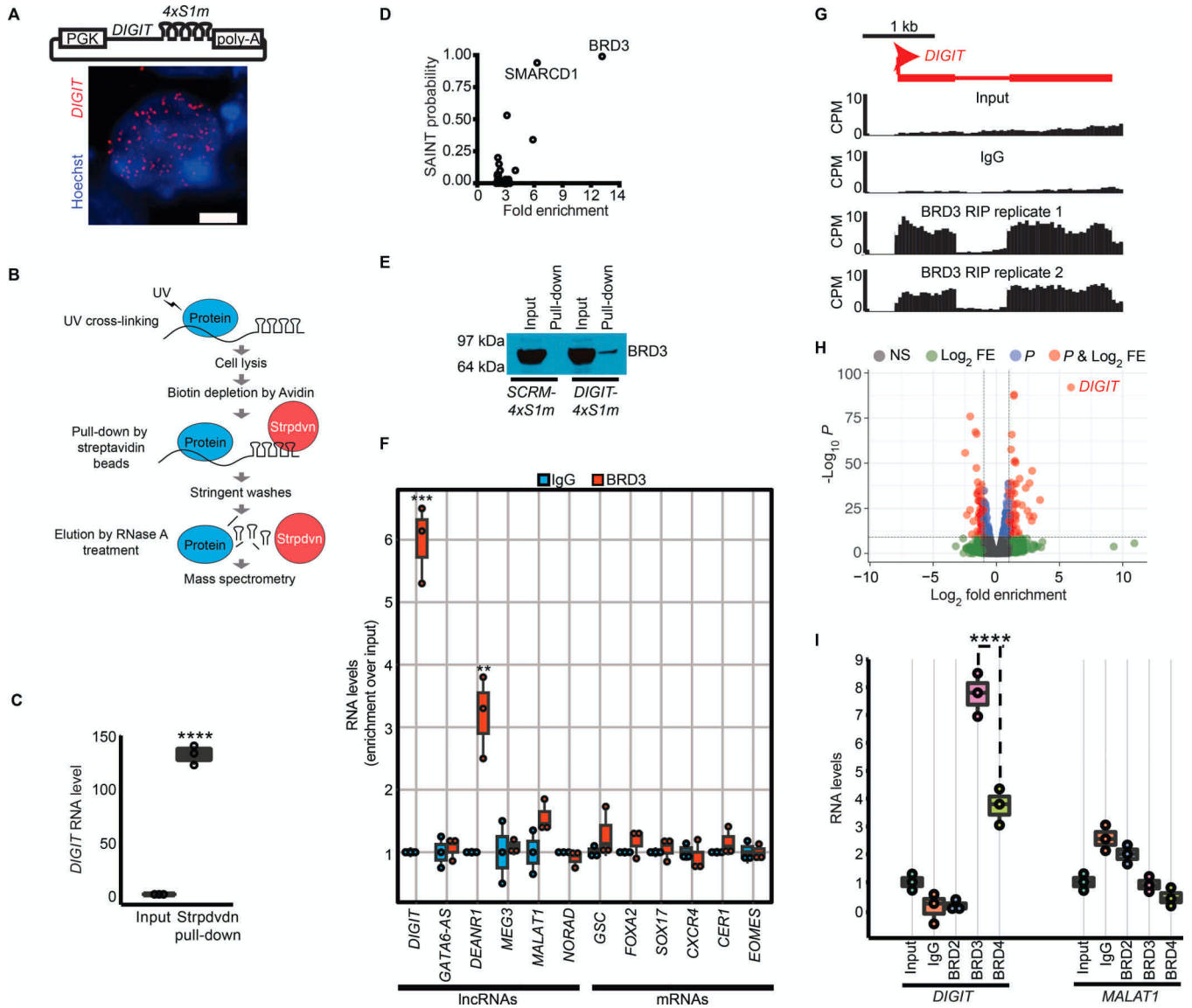
Figure 1. *DIGIT* interacts with BRD3.

(A) Construct expressing *DIGIT* fused to four S1m aptamers (*DIGIT-4xS1m*). Expression is controlled by the Phosphoglycerate kinase 1 promoter and terminated with a polyadenylation sequence. RNA-FISH was performed to detect *DIGIT-4xS1m* in hESCs, where *DIGIT* is not expressed. Similar distribution patterns were observed in 50 nuclei in two independent experiments. The nucleus is shown in blue. Scale bar represents 10 μm. **(B)** Strategy for UV cross-linking, streptavidin pull-down and mass spectrometry (MS). **(C)** *DIGIT-4xS1m* was quantified by qRT-PCR after pull-down. RNA levels are normalized to *GAPDH.* Box plots show the first and third quartiles, median (horizontal line), and minimum and maximum values (whiskers). Circles represent individual data points. **** indicates p <0.0001 (Student's t-test, n=3 independent experiments). **(D)** MS analysis for *DIGIT-4xS1m* compared to *SCRM-4xS1m* and *DIGIT* without aptamers. The probability score represents the SAINT (Significance Analysis of INTeractome) score. This analysis was performed once and was validated by immunoblot. **(E)** Immunoblot for BRD3 was

performed under the indicated conditions. This experiment was performed twice with similar results. **(F)** RIP followed by qRT-PCR was performed in endoderm cells for indicated transcripts. ** indicates p <0.01 and *** indicates p <0.001 (Student's t-test, n=3 independent experiments). Box plots show the first and third quartiles, median (horizontal line), and minimum and maximum values (whiskers). **(G)** RIP followed by RNA sequencing (RIP-seq) results are shown for the *DIGIT* locus. Reads are displayed as counts per million (CPM). **(H)** RIP-seq was performed using an antibody against BRD3 and compared to IgG isotype control. Colors indicate classification of the gene product as showing greater than Log_2 fold enrichment of 1 (Log_2 FE), $-Log_{10}$ of adjusted p-value > 10 (*P*), meeting both criteria (*P*&Log_2 FE), and non-statistically significant enrichment (NS). RIP-seq was performed in two independent samples and pooled for analysis. **(I)** qRT-PCR quantifying *DIGIT* and *MALAT1* (negative control) levels following RIP of the indicated proteins. Enrichment is quantified relative to *GAPDH*. **** indicates p <0.0001 (one-way ANOVA and Tukey's post hoc test, n=3 independent experiments). Unprocessed blots and statistical source data are provided in Source data Fig. 1.

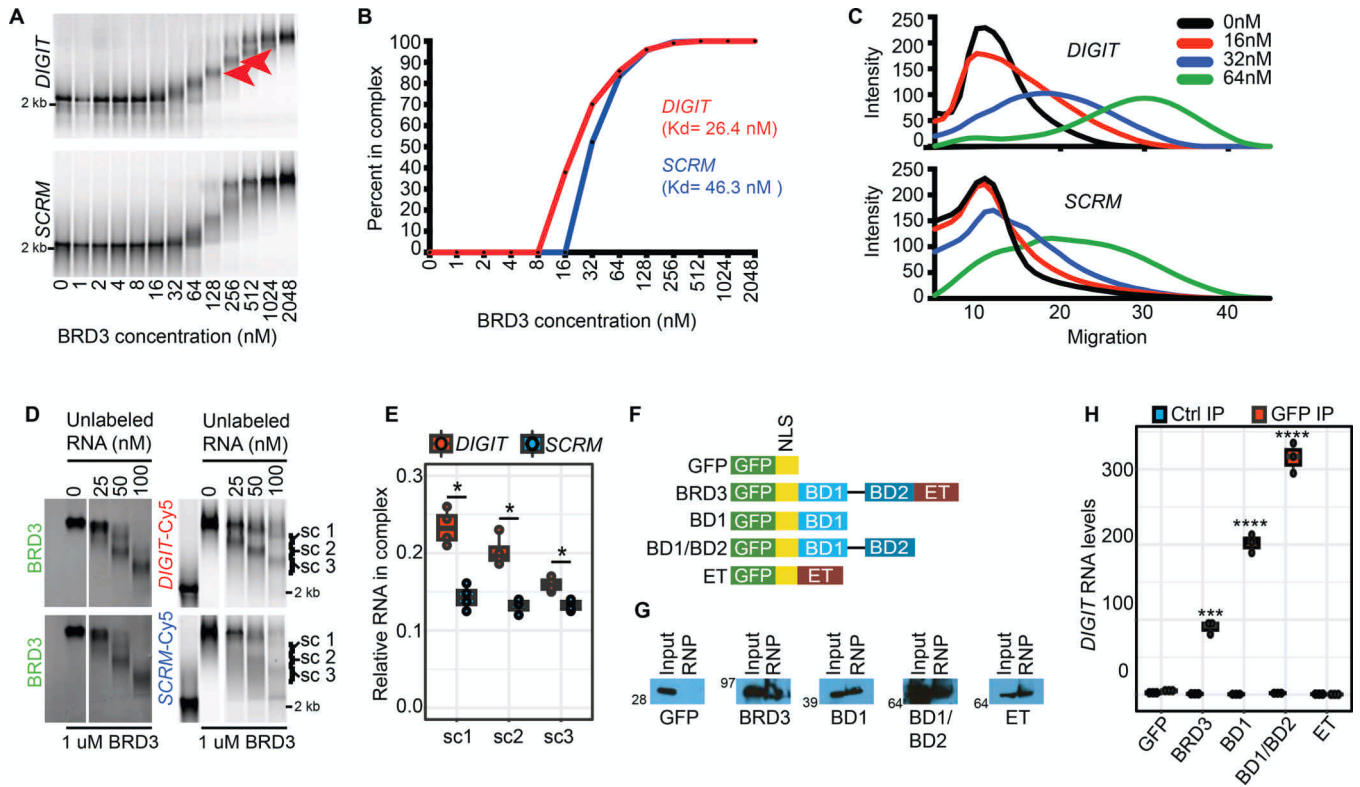**Figure 2. *DIGIT* interacts with recombinant BRD3 in vitro, and bromodomains mediate the interaction between BRD3 and *DIGIT*.**

(**A**) Electrophoretic mobility shift assay (EMSA) of *in vitro* transcribed *DIGIT* (top) and *SCRM* (bottom) with BRD3. *DIGIT* and *SCRM* are labeled with Cy5 and incubated with recombinant BRD3 (long isoform) at the indicated concentrations (x-axis). Red arrows indicate examples of distinct shifted bands. This experiment was repeated three times, independently, with similar results. (**B**) The dissociation constants (Kd) were calculated for Figure 2A. (**C**) Migration was visualized by quantifying the signal for *DIGIT* (top) or *SCRM* (bottom) across the gel in (A). Migration of 0 on the x-axis was defined by the peak of *DIGIT* and *SCRM* with 0 nM BRD3 protein, and migration of 100 was defined by the peak of *DIGIT* and *SCRM* with 2048 nM BRD3 protein. (**D**) Gel electrophoresis shows the accelerated migration of BRD3 with increasing concentrations of RNA (left). *DIGIT* (top, right) migrates more closely with the BRD3 complexes than *SCRM* (bottom, right). 1 uM BRD3-GFP protein and 1nM of labeled (Cy5) RNAs were used for each sample in the presence of increasing concentrations of unlabeled RNAs. Brackets (sc 1, sc 2, sc 3) identify the migration of BRD3 (left) and labeled RNA that migrate with BRD3 (right). (**E**) Quantification of the portion of labeled RNA (sc1, sc2, sc3) from (D) in complex with BRD3. * indicates p<0.05 (Student's t-test, n=4 independent experiments). (**F**) Constructs used in (G). A nuclear localization signal (NLS) is added to GFP to ensure the nuclear retention of all fragments. (**G**) OOPS followed by immunoblotting using an antibody against mEGFP. (**H**) RNA-IP (RIP) followed by qRT-PCR to evaluate the interaction of each construct with *DIGIT*. **** indicates p <0.0001. Box plots show the first and third quartiles, median (horizontal line), and minimum and maximum values (whiskers) and *** indicates p < 0.001 (Student's t-test, n=3 independent experiments). Experiments in (G) and (H) were

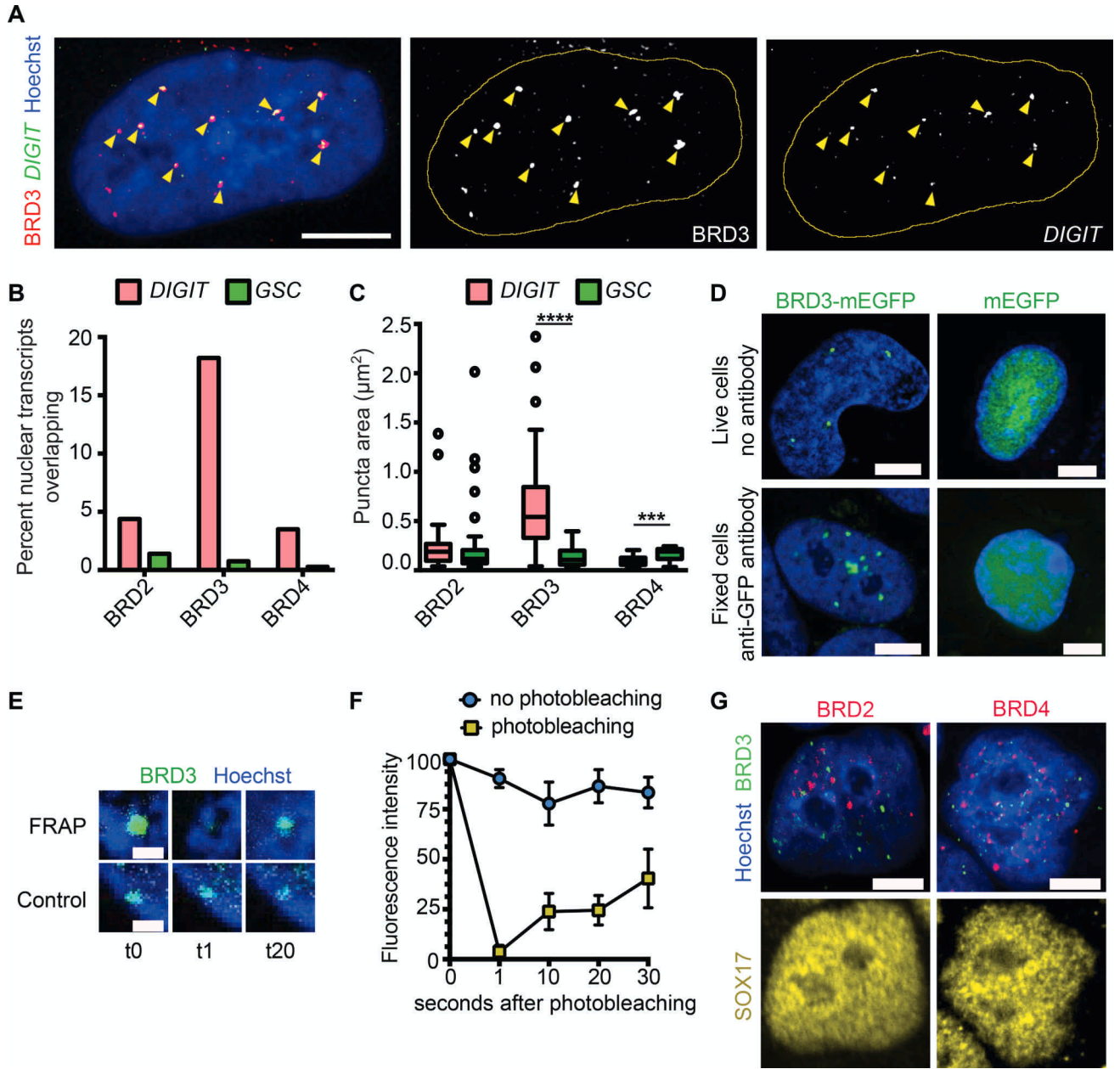performed in 293T cells. Unprocessed blots and statistical source data are provided in Source data Fig. 2.

Figure 3. BRD3 forms protein-RNA phase-separated condensates.
(A) Sequential immunofluorescence and RNA-FISH shows the distribution of BRD3 protein and *DIGIT* RNA within the nucleus on day 4 of endoderm differentiation (left). Areas of overlap are shown in yellow and marked with arrows. The center panel shows BRD3 (white, indicated by arrows) and the right panel shows *DIGIT* (white, indicated by arrows) for the same cell. The nucleus is outlined in yellow for the second and third panel. Scale bar represents 10 μm. The experiment was repeated twice independently. **(B)** The bar chart shows the number of *DIGIT* lncRNA and *GSC* mRNA molecules overlapping with puncta from each BET protein. **(C)** Puncta size is shown for each BET protein that overlaps with *DIGIT* and *GSC*. **** indicates p <0.0001 and *** indicates p < 0.001 (Student's t-test, for BRD2 puncta overlapping with *DIGIT* and *GSC* respectively, n=34 and n=58; for BRD3:

n=69 and n=18; for BRD4: n=30 and n=9 where n=number of puncta containing the indicated transcript after examining more than 50 nuclei in two independent experiments for each category). **(D)** Live (top) and fixed (bottom) fluorescence images of BRD3 condensates are shown in nuclei (blue). BRD3 protein is visualized by creating a fusion protein with mEGFP (Extended Data Figure 4C–D). Scale bar represents 10 μm. This experiment was replicated independently three times. **(E)** FRAP analysis of BRD3 condensates (green) before photobleaching (t0) and 1 second (t1) and 20 seconds (t20) after photobleaching. The analysis was performed on day 4 of endoderm differentiation following the protocol described in Extended Data Figure 1C and 1D. Scale bar represents 1 μm. This experiment was replicated independently twice. **(F)** Quantification of the FRAP experiment (E). Error bars indicate standard deviation calculated from three independent observations in three separated nuclei. Similar results were observed in another replicate of this experiment. **(G)** Co-immunostaining of BRD3 (mEGFP-BRD3) with BRD4 (right) or BRD2 (left) in endoderm cells. Co-staining of SOX17 (bottom panels) is included to mark definitive endoderm cells. Scale bar represents 10 μm. This experiment was repeated independently three times. Statistical source data are provided in Source data Fig. 3.
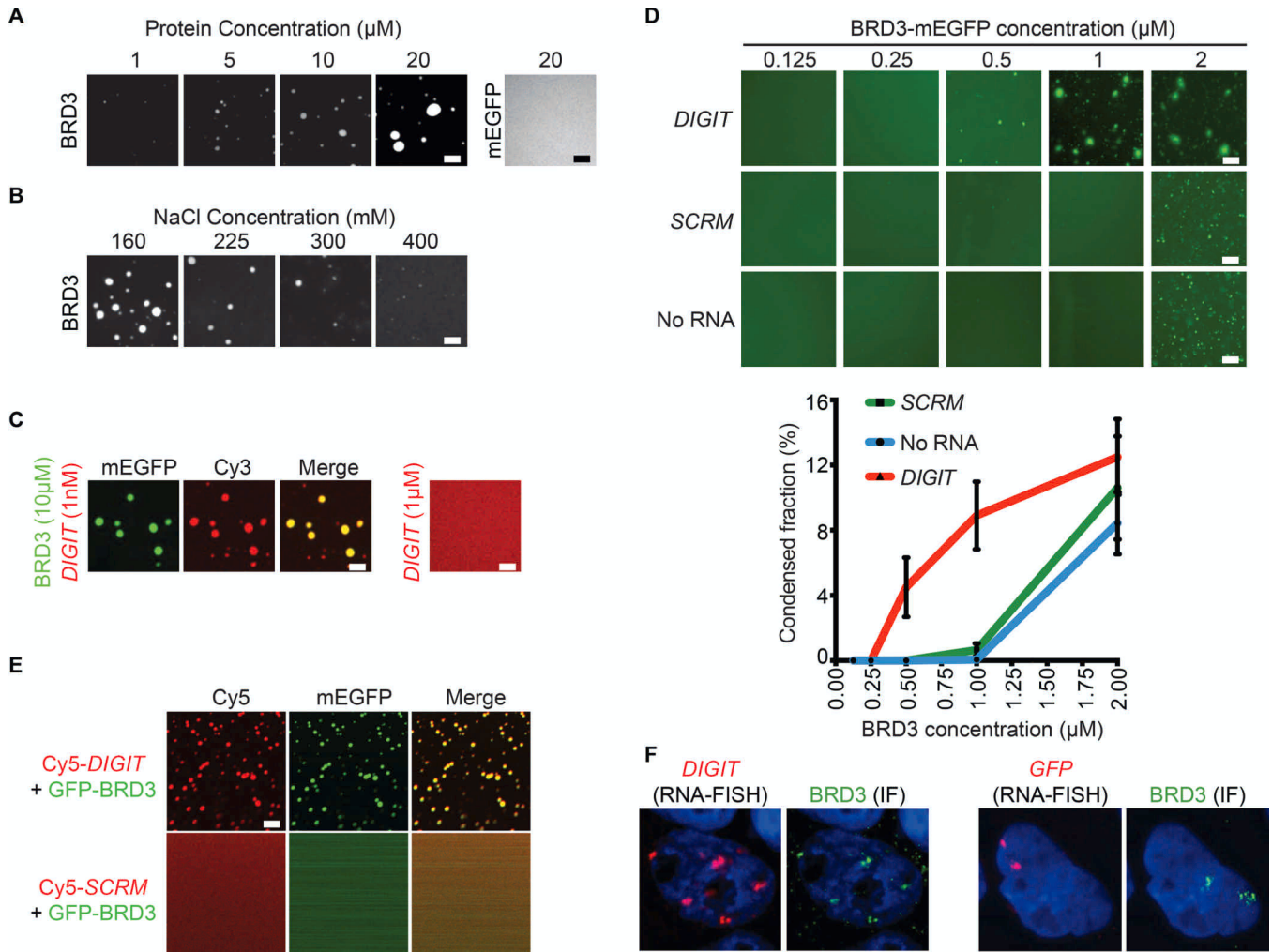
Figure 4. *DIGIT* promotes the formation of BRD3 phase-separated condensates.
(**A**) Purified recombinant BRD3 fused to mEGFP forms phase-separated condensates (white circles on a black background), at the indicated concentrations. Purified recombinant mEGFP is used as control (far right). (**B**) *In vitro* formation of BRD3 condensates as a function of salt concentration. 10 μM BRD3-mEGFP was incubated at the indicated salt concentrations and assessed for droplet formation. (**C**) BRD3 condensates can enrich *DIGIT*. Enrichment of fluorescently labeled *DIGIT* (Cy3, red) within BRD3-mEGFP droplets (green). The overlap between BRD3-mEGFP and *DIGIT*-Cy3 is shown in yellow (Merge). Cy3-*DIGIT* alone is shown on the far right (1 μM) without the formation of any visible condensates. Concentrations of BRD3 and *DIGIT* used for mixing are indicated at the far left. (**D**) Droplet assay shows the formation of mEGFP-BRD3 droplets in the presence of 100 nM *DIGIT* (top row), 100 nM scrambled *DIGIT* (*SCRM*) (middle row), or no RNA (bottom row). The NaCl concentration is 200 mM. 1.5% PEG-6000 was added in each reaction. The bottom plot shows the percent fraction of the total fluorescence that was measured inside the droplets for *DIGIT* (red), *SCRM* (green) and no RNA (blue). Error bars indicate standard deviation of 3 independent experiments. Scale bars in (A-D) represent 2 μm. (**E**) Nucleation of BRD3 droplets in the presence of *DIGIT* but not *SCRM*. Droplet

assay is shown at 1 μM of mEGFP-BRD3 and 100 nM of either *DIGIT* (top panels) or *SCRM* (bottom panels), which were labeled by Cy-5. This experiment was repeated independently three times. **(F)** *DIGIT*-induced nucleation of BRD3 droplets *in vivo*. hESCs stably expressing *DIGIT* (left) or *mEGFP* (right) are shown. BRD3 is detected by immunofluorescence and RNA (*DIGIT* or *mEGFP*) are detected by single-molecule RNA-FISH. The nucleus is shown in blue (Hoechst). Experiments in A, B, C, E and F were repeated three times with similar results. Scale bars in (E) and (F) represent 10 μm. Statistical source data are provided in Source data Fig. 4.
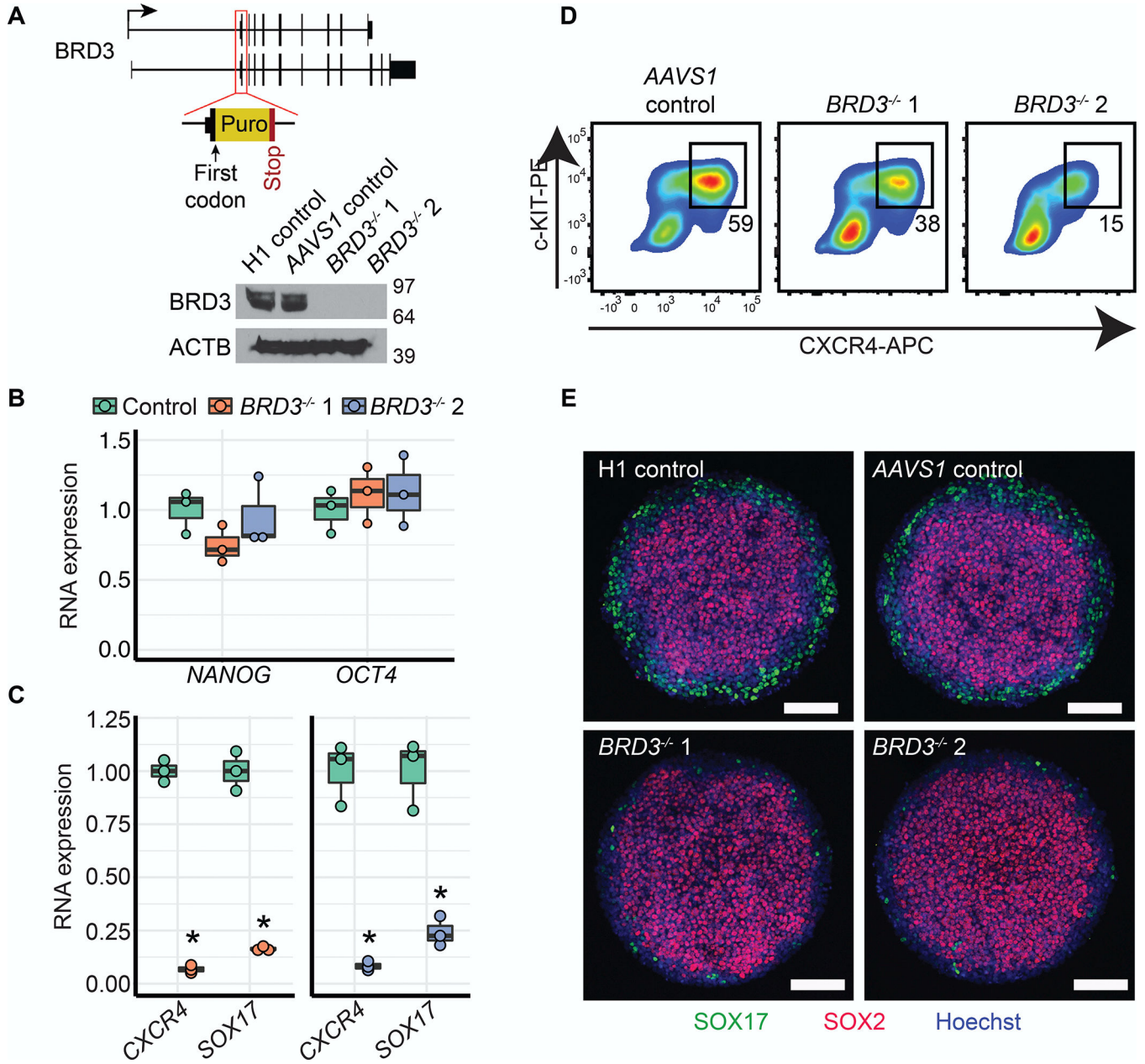
Figure 5. BRD3 regulates endoderm genes.
(A) Strategy for deletion of BRD3 in hESCs using the CRISPR/Cas system and a homology plasmid to insert a puromycin resistance cassette and stop codon into the first coding exon of *BRD3* (top). Immunoblot was performed on cell lysates using an anti-BRD3 antibody. Samples were tested from unmodified H1 hESCs (H1 control), hESCs in which a puromycin cassette was inserted into the *AAVS1* locus (*AAVS1* control), and two independently-derived *BRD3⁻/⁻* lines (1 and 2). ACTB was used as a loading control. **(B)** qRT-PCR was performed to quantify *OCT4* (*POU5F1*) and *NANOG* in *AAVS1* control hESCs and two independently-derived *BRD3⁻/⁻* lines. Colored rectangles represent mean values, and values for each replicate are indicated by open circles. Error bars represent standard deviation. **(C)** qRT-PCR was performed to quantify *SOX17* and *CXCR4* using control hESCs and two

independently-derived *BRD3*$^{-/-}$ lines. Gene expression was analyzed after 4 days of directed differentiation. * indicates p <0.05 (Student's t-test, n=3 independent experiments for *BRD3–/–* 1). Box plots show the first and third quartiles, median (horizontal line), and minimum and maximum values (whiskers). **(D)** Flow cytometry was performed to quantify the expression of CXCR4 and c-KIT in *AAVS1* control hESCs and two independently-derived BRD3$^{-/-}$ lines. The analysis was performed after 4 days of directed endoderm differentiation. Percentages of definitive endoderm cells (boxes) are indicated. **(E)** The indicated hESC lines were differentiated by treatment with BMP4 for 2 days on micropatterned slides. Immunofluorescent staining was performed for SOX2 (red) and SOX17 (green). Nuclei were counterstained with Hoechst (blue). This experiment was repeated twice independently. Scale bar represents 250 μm. Unprocessed blots and statistical source data are provided in Source data Fig. 5.
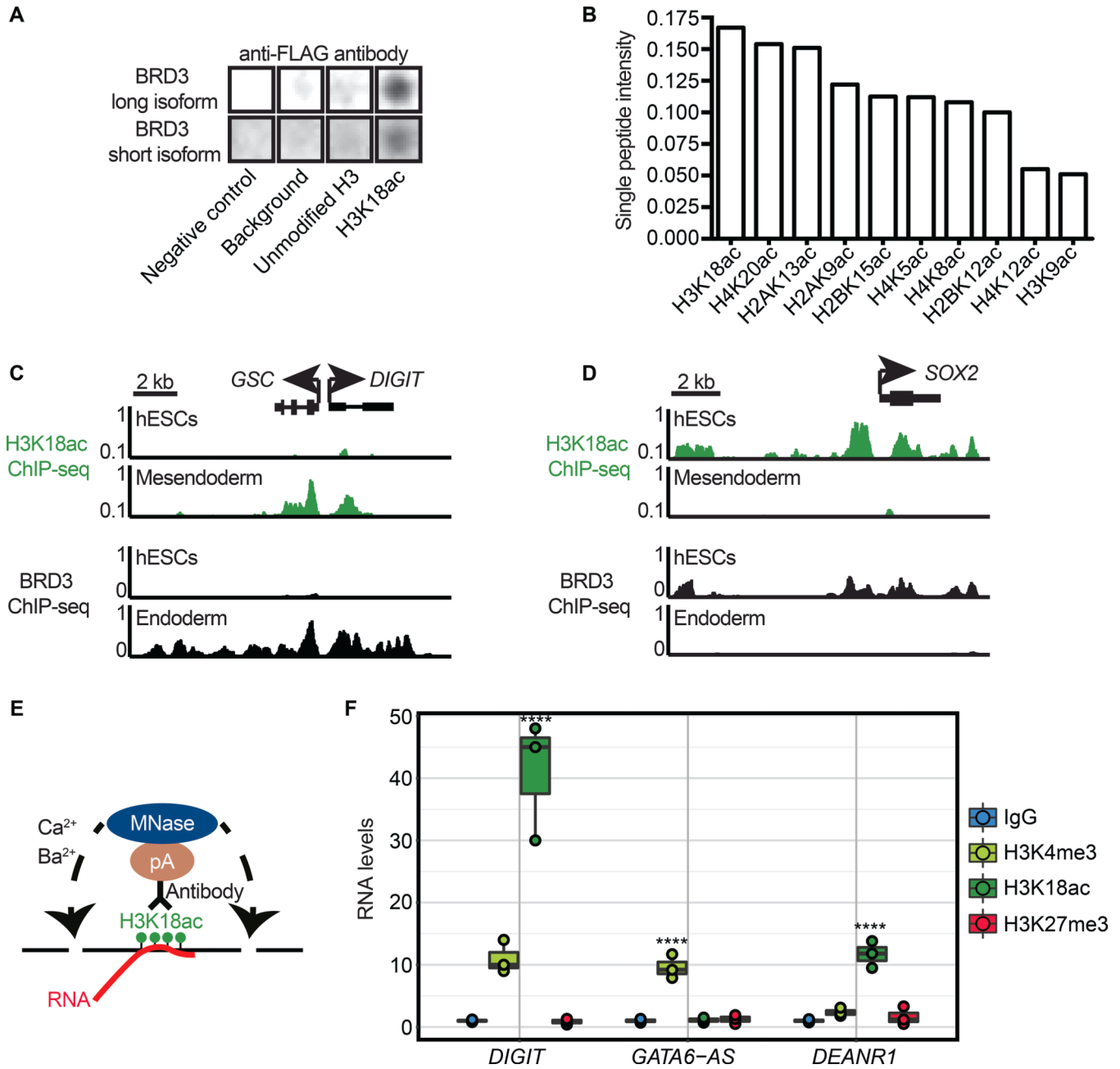
Figure 6. BRD3 and *DIGIT* interact with acetylated H3K18.
(A) Binding of recombinant BRD3 to acetylated H3K18 (H3K18ac) on an array of modified histone peptide modifications. The full arrays are shown in Extended Data Figure 6A. Data are shown for the long isoform of BRD3, which was performed once. Similar results were obtained with the short isoform of BRD3, which was performed twice (Extended data Figure 6A). **(B)** The top 10 modifications bound by recombinant BRD3 protein (long isoform) are shown and ranked in order of single peptide intensity. **(C)** H3K18ac (green) and BRD3 occupancy (black) are shown at the *GSC/DIGIT* locus for hESCs and after mesendoderm (H3K18ac) or endoderm (BRD3) differentiation. The x-axis indicates the linear sequence of genomic DNA, and the y-axis indicates the log number of normalized mapped reads. The

genomic scale in kilobases (kb) is indicated at the top. **(D)** H3K18ac (green) and BRD3 occupancy (black) are shown at the *SOX2* locus. **(E)** Schematic showing the strategy for CUT&RUNER, which takes advantage of targeted digestion of chromatin fragments using Protein A (pA) fused MNase followed by isolation of the released chromatin-bound RNA. The presence of barium (Ba^{2+}) inhibits the RNase activity of MNase. Calcium (Ca^{2+}) is required for the enzymatic activity of MNase. Arrows indicate sites of DNA cleavage by MNase. **(F)** qRT-PCR shows the levels of *DIGIT* (left), *GATA6-A6* (center), and *DEANR1* (right) isolated by performing CUT&RUNER with antibodies recognizing the indicated chromatin modifications in hESCs differentiated toward definitive endoderm. RNA levels are normalized to *GAPDH* expression. IgG is used as a negative antibody control. **** indicates $p < 0.0001$ (one-way ANOVA and Tukey's post hoc test, n=3 independent experiments) and error bars represent standard deviation. Unprocessed blots and statistical source data are provided in Source data Fig. 6.
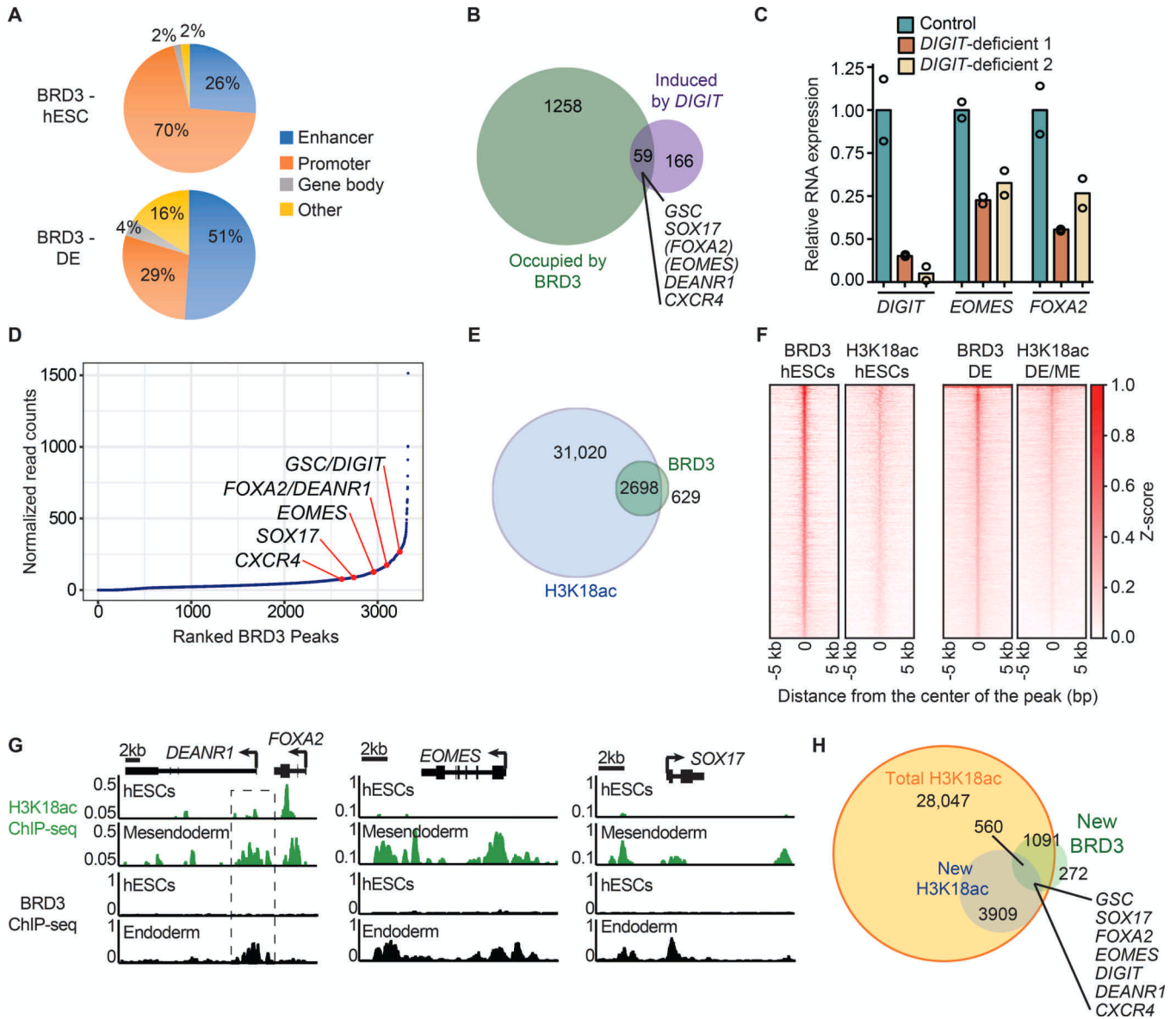
Figure 7. BRD3 interacts with *DIGIT*-regulated genes on H3K18ac-marked chromatin.
(A) The percentage of BRD3 regions in each category is indicated for 1445 regions in hESCs and 3327 regions in DE. Data from two independent BRD3 ChIPs were pooled for analysis of hESCs and DE. **(B)** Overlap of genes occupied by BRD3 and repressed with depletion of *DIGIT* (induced by *DIGIT*) during endoderm differentiation. The p-value of the overlap as calculated by Fisher's exact test is 3.2×10^{-11}. Endoderm genes that are regulated by *DIGIT* and occupied by BRD3 are listed. Genes in parentheses did not meet statistical significance on RNA-seq (FDR <0.01)[4] and were validated by qRT-PCR in (C). Data from two independent BRD3 ChIPs were pooled for analysis. **(C)** qRT-PCR was performed after endoderm differentiation of two independently-derived *DIGIT*-deficient hESCs lines[4]. RNA expression is normalized to 1.0 in control cells. Colored rectangles represent mean values. Open circles indicate the values for each replicate. **(D)** Regions of BRD3 occupancy in endoderm cells are ordered from the lowest to highest BRD3 read counts (Ranked BRD3

peaks). Endoderm genes are labeled in red. Data from two independent BRD3 ChIPs were pooled for analysis. **(E)** The overlap of regions modified by H3K18ac in mesendoderm and occupied by BRD3 in endoderm is shown. Data from two independent BRD3 ChIPs were pooled for analysis and compared to H3K18ac[43]. **(F)** Heatmaps show co-occupancy of BRD3 and H3K18ac in hESCs and endoderm/mesendoderm (DE/ME). Data from two independent BRD3 ChIPs were pooled for analysis. H3K18ac ChIP-seq analysis was performed on mesendoderm[43]. **(G)** Genes modified by H3K18ac and occupied by BRD3 upon differentiation of hESCs toward mesendoderm and endoderm. The dotted box indicates the region of overlap between H3K18ac and BRD3 near *FOXA2* and *DEANR1.* **(H)** Regions modified by H3K18ac in mesendoderm, newly modified by H3K18ac with mesendoderm differentiation, and newly occupied by BRD3 with endoderm differentiation. The intersection of regions newly modified H3K18ac and BRD3 contains the indicated endoderm factors. Data from two independent BRD3 ChIPs were pooled for analysis and compared to H3K18ac[43]. Statistical source data are provided in Source data Fig. 7.
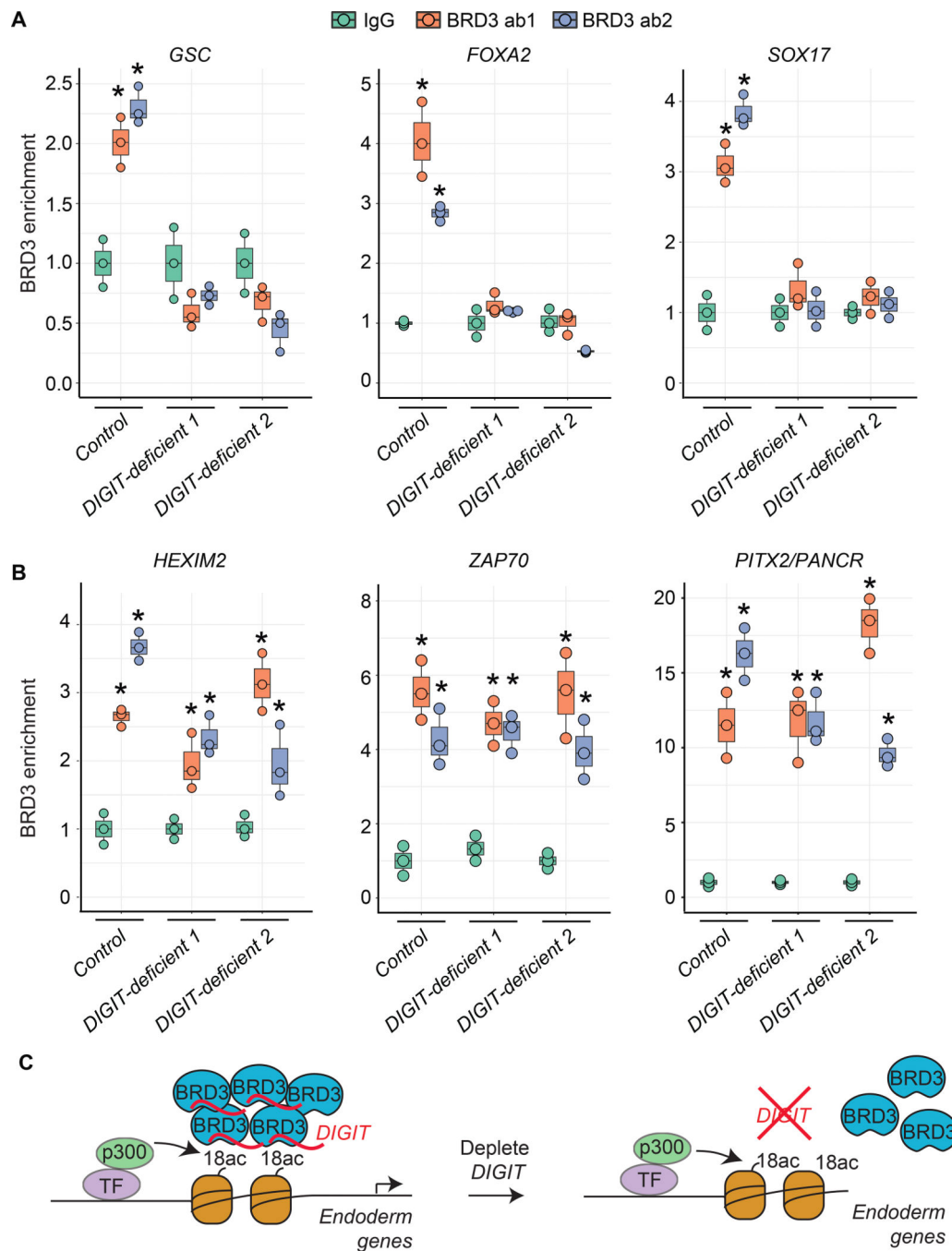
Figure 8. Loss of *DIGIT* inhibits the recruitment of BRD3.

(**A**) CUT&RUN was performed followed by qPCR to quantify the enrichment of BRD3 at the *GSC* (left), *FOXA2* (center), and *SOX17* loci (right). Chromatin release was directed using two antibodies recognizing BRD3 (ab1 and ab2). Two independently-derived *DIGIT*-deficient lines (*DIGIT$^{gfp/gfp}$*) were used for each experiment. Error bars represent standard deviation. * indicates $p < 0.05$ (one-way ANOVA and Tukey's post hoc test, n=3 independent experiments), compared to IgG. (**B**) CUT&RUN was performed as in (A) using primers that recognize *HEXIM2* (left), *ZAP70* (center), and *PITX2/PANCR* (right). * indicates $p < 0.05$

(one-way ANOVA and Tukey's post hoc test, n=3 independent experiments), compared to IgG. Box plots show the first and third quartiles, median (horizontal line), and minimum and maximum values (whiskers). **(C)** Schematic showing condensates of BRD3 and *DIGIT* interacting with H3K18ac (18ac) to induce endoderm gene expression. H3K18 is acetylated by CBP/p300 (p300) following recruitment by transcription factors (TF)[34,72]. In the absence of *DIGIT,* BRD3 is not able to bind to H3K18ac in this region, and the endoderm gene is not activated. Statistical source data are provided in Source data Fig. 8.